

Tuning nonthermal distributions to thermal ones in time-dependent Paul traps

H. Landa^{1*}

¹*Institut de Physique Théorique, Université Paris-Saclay, CEA, CNRS, 91191 Gif-sur-Yvette, France*

We study the probability distribution of an atomic ion being laser-cooled in a periodically-driven Paul trap using a Floquet approach to the semiclassical photon scattering dynamics. We show that despite the microscopic nonequilibrium forces, a stationary thermal-like exponential distribution can be obtained in the Hamiltonian action, or equivalently in the number of quanta (phonons) of the motion linearized about the zero of the potential. At the presence of additional stray electric fields, the ion is pushed from the origin of the potential and set into a large-amplitude driven oscillation, and above a threshold amplitude of such “excess micromotion”, the action distribution of excitations about the driven oscillation broadens and becomes distinctly nonthermal. We find that by a proper choice of the laser detuning the distribution can be made exponential again, with a mean phonon number close to that of the Doppler cooling limit. We derive a relation allowing to deduce just from the experimentally observable photon scattering rate both the required detuning for optimal cooling and the final mean phonon number. These results are important for quantum information processing and other applications, and in particular the derived approach can be applied to crystals of trapped ions in planar configurations, where the driven motion of ions is unavoidable.

I. INTRODUCTION AND MAIN RESULTS

A most common method of trapping charged particles in vacuum is by use of electrodynamic Paul traps [1]. The electric potential generated in these traps is time-dependent, as the applied electrode voltages are periodically modulated at a radio-frequency (rf) rate. Close enough to the effective potential minimum in many Paul trap variants, the potential is well approximated by a quadrupole term, bilinear in the coordinates. A periodically-driven quadrupole potential gives rise to time-dependent, linear, Mathieu equations of motion. The motion of the ions is then characterized by quasi-periodic harmonic oscillations at the so-called “secular” frequencies, superimposed with the fast “micromotion” driven by the time-dependent potential. Since the equations of motion are integrable (being linear), the description of the motion can be simplified using classical action-angle coordinates. For a given initial condition, the trajectory in the phase-space of coordinates and momenta is restricted to rotations on an invariant manifold. This is a torus whose dimension is half that of the phase-space. The ion’s position on the torus at any time is given by the angles which are the generalized coordinates, each evolving independently and increasing linearly in time (with a fixed angular frequency). The measure within the torus (the bounded hyper-volume in the phase-space) is determined by the actions which in the absence of perturbations are conserved quantities of the motion.

An important tool employed to control the dynamics of an ion and break the conserved quantities is laser cooling, a well established method for removing entropy, e.g. from a trapped ion’s motion [2–14]. A stochastic process by

its very nature, laser cooling is based on the absorption of photons with a narrow momentum bandwidth determined by the laser, followed by a spontaneous emission of photons with randomly directed momenta.

In this work we use a recently developed semiclassical framework for studying laser cooling dynamics of ions driven by micromotion up to large amplitudes of motion [15]. We focus on a single ion’s distribution in the final stage of the cooling. Since the Paul trap potential is time-dependent, the distribution function in the positions and velocities is non-stationary; it is periodic with the period of the trap [8]. A key idea underlying the current treatment is that by using the action that is a time-independent quantity, the periodic, driven component in the kinetic energy is readily separated from the stochastic component. In terms of the action it is easy to distinguish an effective, stationary thermal-like exponential distribution from other, nonthermal and much more broad distributions possible for the ion in the final stage of Doppler cooling. Such nonthermal distributions arise due to the photon scattering dynamics being modified by a large-amplitude driven motion of the ion, as analyzed in the following.

In order to describe periodically driven photon scattering processes we derive in Sec. II B, using a Floquet approach, a new solution of the Optical Bloch Equations (OBE) for a two-level system. This Floquet expansion allows us to account accurately for the micromotion, and it can be used quite generally [16]. In Sec. III we introduce the setup that is studied in detail in this work, of an ion being laser-cooled in a region of a Paul trap where the potential is approximately a quadrupole potential. We present analytic and numerical results for the simplified case of one-dimensional (1D) motion, with the detailed derivations for three-dimensional (3D) motion left for the Appendix (see below). In Sec. IV A we review the Fokker-

* haggaila@gmail.com

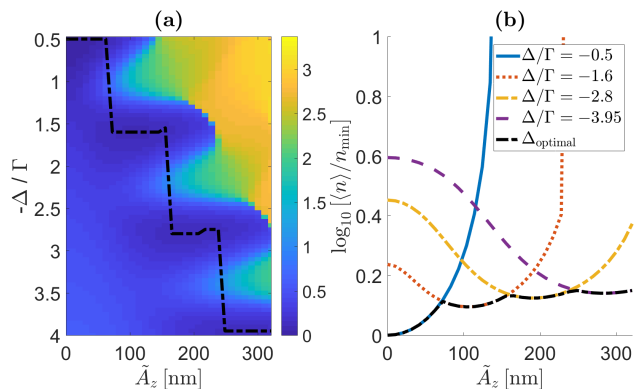


FIG. 1. (a) The mean steady-state phonon number $\langle n \rangle$ [Eq. (61)] as a function of the laser detuning Δ (in units of the natural linewidth of the cooling transition, Γ), and the excess micromotion amplitude \tilde{A}_z [Eq. (2), given in nanometers for the presented parameters], for one coordinate (z) of a $^{24}\text{Mg}^+$ ion being laser cooled within a linear Paul trap potential with the frequencies given in Eq. (1). The color code indicates the base-10 logarithm of $\langle n \rangle$, in units of the Doppler cooling limit phonon number n_{\min} , attainable in the upper left corner of the plot, for $\Delta = -\Gamma/2$ and $\tilde{A}_z = 0$, and up to ~ 3 orders of magnitude larger. The dashed-dotted black line gives the function $\Delta_{\text{optimal}}(\tilde{A}_z)$ that determines an optimal detuning as function of \tilde{A}_z , for which $\langle n \rangle$ can be reduced to a minimum. (b) Curves obtained from the map of panel (a), showing the attainable minima of the final excitation as a function of the excess micromotion amplitude. Here the vertical axis is truncated at 1, corresponding to $\langle n \rangle = 10 \times n_{\min}$.

Planck (FP) framework for laser cooling that is the main tool employed in this work. This approach is based on the observation that for typical laser cooling rates we can consider the motion as Hamiltonian over a large number of rotations on the invariant torus, and the laser can be modelled as acting on the action alone (with the angles averaged over). The effect of the laser is then to permit the ion to drift and diffuse between the invariant tori of the Hamiltonian phase-space, described by using a Fokker-Planck equation for the probability distribution of the ion in terms of the action.

The probability distribution in the final stage of Doppler cooling is known to be thermal for an ion within a time-independent harmonic trap [3]. As presented in Sec. IV C, we show that even with periodically-driven dynamics where the ion accelerates between the photon absorption and the spontaneous emission, a nearly identical, exponential distribution is obtained with a mean action corresponding to the Doppler limit. Extending the theory to include stray electric fields which may push the ion away from the origin of the quadrupole potential, leading to “excess micromotion” [17–19], detailed numerical calculations are presented in Sec. V. Considering motion in 1D along the z coordinate, taken to be a (micromotion-driven) coordinate within a quadrupole

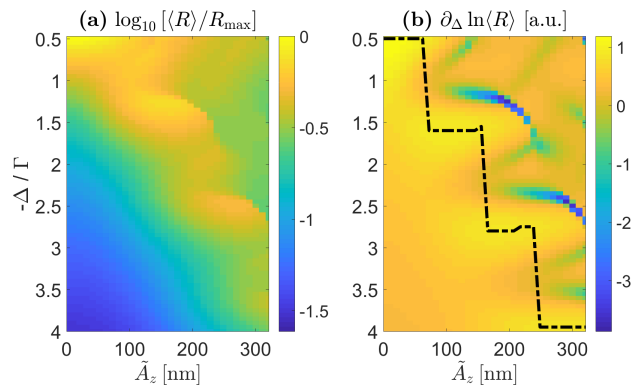


FIG. 2. (a) The mean photon scattering rate $\langle R \rangle$ [Eq. (62)] as a function of the detuning and the excess micromotion amplitude as in Fig. 1. The color code indicates the base-10 logarithm of $\langle R \rangle$, in units of the maximal scattering rate R_{\max} , attainable in the upper left corner of the plot, for $\Delta = -\Gamma/2$ and $\tilde{A}_z = 0$. (b) The logarithmic derivative (with respect to the detuning) of the mean scattering rate mapped in panel (a). The dashed-dotted black line follows the maximum $\max_{\Delta} [\partial_{\Delta} \ln \langle R \rangle]$ at each \tilde{A}_z value. This experimental observable gives immediately both the optimal detuning curve $\Delta_{\text{optimal}}(\tilde{A}_z)$ shown in Fig. 1, along which the ion is cooled to a thermal distribution with minimal width. The value of $\langle n \rangle$ along this curve can be obtained as well (see Fig. 3).

Paul trap, we study laser cooling in the low-saturation (low laser intensity) limit. We present results in three different regimes of the micromotion frequency – low, comparable and high, with respect to the linewidth Γ of the electronic transition driven by the laser, approximated as a two-level system.

To summarize the main results of the current study, we consider cooling of a $^{24}\text{Mg}^+$ ion with trap and laser parameters as detailed in Eqs. (89)-(92). The rf-drive (micromotion) frequency taken here and the oscillator’s secular frequency [Eq. (46)] are

$$\Omega = 2\pi \times 50 \text{ MHz}, \quad \omega_z \approx 2\pi \times 2.8 \text{ MHz}. \quad (1)$$

The ion’s z motion is expanded in the following form

$$\tilde{z}(t) = \tilde{A}_0 + \frac{1}{2} \tilde{A}_z \cos(\Omega t) + \tilde{u}(t), \quad (2)$$

with \tilde{A}_0 the ion’s mean position, \tilde{A}_z the amplitude of the excess micromotion oscillation, and $\tilde{u}(t)$ the motion expanded about the driven oscillations, which is the free degree of freedom being cooled by the laser. We calculate the steady-state of the laser cooled ion when varying two parameters – the laser detuning Δ with respect to the resonant rest-frame electronic transition frequency, and the amplitude of the driven excess micromotion oscillations, \tilde{A}_z (reaching 300 nm for a stray electric field along z of magnitude $\sim 150\text{V/m}$).

Figure 1 shows the mean excitation of the linear oscillator corresponding to the ion’s motion, measured in

terms of the equivalent mean phonon number n by using the semiclassical relation [see Eq. (A23)]

$$n \approx I/\hbar, \quad (3)$$

where I is the classical action for the linearized motion [$\tilde{u}(t)$], \hbar is Planck's constant, and the zero-point motion [$+1/2$ on the left of Eq. (3)] has been neglected. At a fixed value of Δ , a large excess micromotion amplitude could lead to a large phonon number in the steady-state. However, at each fixed excess micromotion amplitude, an optimal value of the detuning (given by $\Delta_{\text{optimal}}(\tilde{A}_z)$ and depicted by a dashed-dotted line), can be chosen for which the mean excitation is reduced to a minimal value close to the Doppler cooling limit n_{min} obtained for $\Delta = -\Gamma/2$ and $\tilde{A}_z = 0$.

Noticeable ‘‘tongues’’ can be seen in Fig. 1, at intervals obeying $-\Delta = m\Omega$ with m a natural number, i.e. at the intervals $-\Delta/\Gamma \approx 1.2m$. Since the chosen micromotion frequency is comparable in magnitude to $\Gamma/2$, we account for the photon absorption probability by using a Floquet solution to the periodically-driven OBE equations [Eq. (67)], and the tongues can be attributed to parametric resonances (see also App. D). A brief analysis of the nonmonotonous features of the curves seen in Fig. 1(b) is presented in Sec. V A, where we study cooling when approaching the limit of a low micromotion frequency. A further look into the role of the Floquet resonances is presented in Sec. V B, where the limit of a high micromotion frequency is analyzed.

Figure 2(a) shows the mean photon scattering rate $\langle R \rangle$ [defined in Eq. (62)] in the steady-state calculated in Fig. 1. The importance of this observable which can be straightforwardly measured experimentally is in giving access to both $\Delta_{\text{optimal}}(\tilde{A}_z)$ and $\langle n \rangle$ along this optimal cooling curve. As shown in Sec. IV D, the maximum $\max_{\Delta} [\partial_{\Delta} \ln \langle R \rangle]$ of the logarithmic derivative (with respect to the detuning) of $\langle R \rangle$ at each fixed \tilde{A}_z value, is obtained along the curve $\Delta_{\text{optimal}}(\tilde{A}_z)$ that can hence be readily reconstructed experimentally. In addition, the mean phonon number along this curve can be approximated using the simple formula

$$\langle n \rangle \approx [\partial_{\Delta} \ln \langle R \rangle]^{-1} \tilde{n}, \quad (4)$$

where \tilde{n} is a proportionality constant defined in Eq. (88), which depends only on the trap and laser parameters.

Figure 3(a) shows a few probability distribution curves for the phonon number with $\tilde{A}_z = 145$ nm and varying values of the detuning. From clearly nonthermal (and even multi-peaked) distributions at low detuning, exponential (thermal-like) distributions can be obtained by increasing the detuning. As can be seen in Fig. 3(b), along the optimal detuning curve a mean phonon number larger than the minimal value at the Doppler cooling limit by only 1-2 quanta is obtainable for any excess micromotion amplitude.

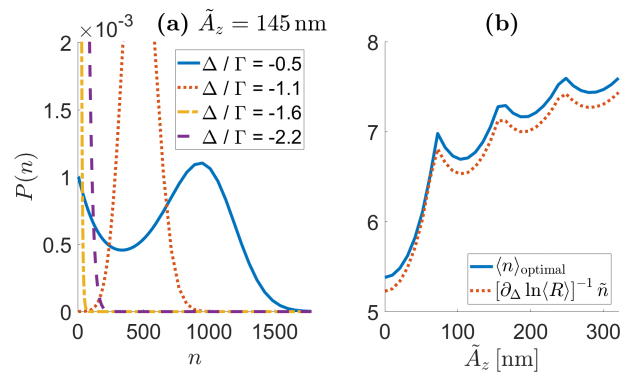


FIG. 3. (a) The stationary probability distribution as a function of the phonon number for $\tilde{A}_z = 145$ nm and different values of the detuning Δ , with the laser and trap parameters as in Fig. 1. For $\Delta = -0.5\Gamma$ and $\Delta = -1.1\Gamma$ the distribution is clearly nonthermal. For $\Delta = -1.6\Gamma$ the distribution is exponential (thermal-like) and with the minimal achievable mean phonon number. For higher detunings the distribution broadens (but remains exponential). (b) The optimal mean phonon number as a function of the excess micromotion amplitude [for a detuning chosen along $\Delta_{\text{optimal}}(\tilde{A}_z)$], depicted by the solid blue line. The dashed red line gives the optimal mean phonon number as obtained from Eq. (4) which can be directly calculated from the observed photon scattering rate.

Thus we find that Δ can be used as a control parameter to counteract, to a high extent, the effect of excess micromotion. As shown in [15], increasing Δ is also efficient for cooling the ion from the regime of approximately integrable high amplitude motion in the anharmonic potential of a surface-electrode trap with a high micromotion frequency, wherein a low-detuning laser (with $\Delta \approx -\Gamma/2$) may more easily heat the ion past the trap barrier. We also show in Sec. V B that such a low-detuning laser may not be efficient in cooling the ion at the presence of stray electric fields and large excess micromotion. However, it should be noted that a laser beam with a large detuning could actually capture the ion in a large amplitude motion away from the trap centre, when chaotic motion becomes significant in the phase space [21].

We conclude with a brief summary and an outlook for possible applications and generalizations in Sec. VI. In the Appendix, we lay down the details of the action-angle treatment of a coupled system of Mathieu oscillators. The exact action-angle coordinates (derived in App. A) can be used for obtaining the FP coefficients for 3D motion of a single ion within quadrupole traps. The derived expressions can be applied to the linearized oscillations of a crystal of trapped ions about their minimum positions [22]. Closed form expressions are derived for Doppler cooling in the linear limit (App. B). Some derivations of the 1D results presented within the main text of the paper are given in App. C, and App. D connects our approach with earlier results in the field [17–19].

II. THE OPTICAL BLOCH EQUATIONS

A. Derivation

In this subsection we review the derivation of the Optical Bloch Equations (OBE) following [23]. A monochromatic laser in a travelling-wave configuration can be described by a classical electric field of the form

$$\vec{E}_L(\vec{r}, t) = E_L \hat{e} \cos(\omega_L t - \vec{k} \cdot \vec{r} + \phi_L), \quad (5)$$

where E_L is the electric-field amplitude, \hat{e} the unit-vector of its polarization, \vec{k} its wavevector, $\omega_L = |\vec{k}|/c$ its frequency, ϕ_L the optical phase, and \vec{r} the ion's position vector. The OBE for a two-level system describe the time evolution of the elements of the density matrix of the two-level system approximating the electron, subject to the driving by the laser and to spontaneous emission. The electronic levels are the ground-state $|g\rangle$ with zero energy and the excited level $|e\rangle$, with an electronic transition between the two of frequency ω_e . The OBE are derived in the long-wavelength approximation, such that the laser wavelength is much larger than the atomic size. The two-level Hamiltonian is

$$H_e = \hbar\omega_e |e\rangle \langle e| + \hbar\Omega_R \cos(\omega_L t + \phi) [|g\rangle \langle e| + |e\rangle \langle g|], \quad (6)$$

where Ω_R is the Rabi frequency (proportional to E_L and to the matrix element of the electric dipole transition), and

$$\phi = \phi(\vec{r}) = -\vec{k} \cdot \vec{r}(t) + \phi_L, \quad (7)$$

depends on the ion's position in configuration space.

The density-matrix of the two-level system evolves subject to the Hamiltonian of Eq. (6), and with spontaneous emission described by Lindblad-type terms. The master equation, in the rotating-wave approximation, can be written in terms of the four matrix elements σ_{ab} , with $a, b \in \{g, e\}$, which gives the OBE in the form

$$\dot{\sigma}_{ee} = -\Gamma\sigma_{ee} - i\frac{\Omega_R}{2} (e^{-i\omega_L t - i\phi} \sigma_{ge} - e^{i\omega_L t + i\phi} \sigma_{eg}), \quad (8)$$

$$\dot{\sigma}_{ge} = \left(i\omega_e - \frac{\Gamma}{2}\right) \sigma_{ge} - i\frac{\Omega_R}{2} e^{i\omega_L t + i\phi} (\sigma_{ee} - \sigma_{gg}), \quad (9)$$

where $\sigma_{ge} = \sigma_{eg}^*$ and from the density matrix having unit trace we get $\sigma_{gg} + \sigma_{ee} = 1$, which implies $\sigma_{ee} - \sigma_{gg} = 2\sigma_{ee} - 1$. Hence Eqs. (8)-(9) form a closed system, that depends on the (semiclassical) dynamics of the ion through the variation of the phase of Eq. (7). It can be seen that the off-diagonal terms σ_{ge} and σ_{eg} decay at a rate $\Gamma/2$, while the diagonal terms decay with rate Γ , where Γ is the spontaneous emission rate (the linewidth of the transition).

Substituting into Eq. (9) the new variable

$$\sigma'_{ge} = e^{-i\omega_L t - i\phi[\vec{r}(t)]} \sigma_{ge}, \quad (10)$$

we get after rearranging, the modified OBE

$$\dot{\sigma}_{ee} = -\Gamma\sigma_{ee} - i\frac{\Omega_R}{2} (\sigma'_{ge} - \sigma'_{eg}), \quad (11)$$

$$\dot{\sigma}'_{ge} = \left[-i\left(\Delta - \vec{k} \cdot \vec{v}\right) - \frac{\Gamma}{2}\right] \sigma'_{ge} - i\frac{\Omega_R}{2} (2\sigma_{ee} - 1), \quad (12)$$

with the detuning $\Delta = \omega_L - \omega_e$ and the velocity $\vec{v} = \dot{\vec{r}}$.

When \vec{v} can be assumed to evolve slowly on the scale of $\Gamma/2$, the steady-state of the coupled OBE can be found by setting the time-derivatives to 0, and σ_{ee} , which is the mean probability of the electron to be found in the excited level, obtains a well-known Lorentzian form in the velocity [15] with the saturation accounted for).

B. Low-saturation solution with a Floquet approach

To proceed we now consider the low saturation limit (low laser intensity, or a solution to leading (second) order in Ω_R),

$$s = 2(|\Omega_R|/\Gamma)^2 \ll 1. \quad (13)$$

In this limit, we assume that the solution obeys $\sigma_{ee} \ll 1$ and write in Eq. (12), $2\sigma_{ee} - 1 \approx -1$. Then, Eq. (12) decouples to become

$$\dot{\sigma}'_{ge} = \left[-i\Delta_{\text{eff}}(t) - \frac{\Gamma}{2}\right] \sigma'_{ge} + i\frac{\Omega_R}{2}, \quad (14)$$

where we have defined

$$\Delta_{\text{eff}}(t) = \Delta - \vec{k} \cdot \vec{v}(t). \quad (15)$$

The general solution of Eq. (14) consists of the sum of a transient solution to the homogeneous part of the equation which will decay with an exponential envelope of $e^{-\Gamma t/2}$, and a particular solution to the inhomogeneous Eq. (14) which gives the steady-state. The solutions can be obtained in closed-form by integration, however, it is instructive to use a Floquet approach to analyze the steady-state solution.

Let us assume that the velocity (along the laser wavevector) is periodic in time with Ω the fundamental frequency of the periodic motion. Using the nondimensional units given in App. A, we set $\Omega = 2$ obtained by rescaling

$$t \rightarrow \Omega t/2 \quad (16)$$

and measuring accordingly all frequency quantities in units of $\Omega/2$, and hence we can write

$$-i\Delta_{\text{eff}}(t) - \frac{\Gamma}{2} = \sum_n D_{2n} e^{i2nt}. \quad (17)$$

The particular non-transient solution to the inhomogeneous Eq. (14) which is periodic with the parametric drive can be written using a Floquet expansion as

$$\sigma'_{ge} = \sum_n G_{2n} e^{i2nt}, \quad (18)$$

with coefficients G_{2n} that will be determined in the following. Substitution in Eq. (11) gives

$$\dot{\sigma}_{ee} = -\Gamma\sigma_{ee} + \Omega_R \text{Im} \left(\sum_n G_{2n} e^{i2nt} \right), \quad (19)$$

whose particular periodic solution takes the form

$$\begin{aligned} \sigma_{ee} &= \Omega_R e^{-\Gamma t} \sum_n \int_0^t \text{Im} \left(G_{2n} e^{(\Gamma+i2n)t'} \right) dt' = \\ &= \sum_n \frac{\Omega_R}{\Gamma^2 + (2n)^2} \text{Im} \left(G_n (\Gamma - i2n) e^{i2nt} \right). \end{aligned} \quad (20)$$

The Floquet expansion coefficients G_{2n} can be found using known methods. In the important case of a simple harmonic and time-reversal invariant Δ_{eff} , we can use known expressions for an inhomogeneous driven Mathieu oscillator [24]. We assume the following expansion for Eq. (17),

$$-i\Delta_{\text{eff}}(t) - \frac{\Gamma}{2} = D_0 - 2D_2 \cos(2t), \quad (21)$$

and substitute in Eq. (14) to obtain

$$\begin{aligned} -i \sum_n 2n G_{2n} e^{i2nt} + \\ [D_0 - D_2(e^{i2t} + e^{-i2t})] \sum_n G_{2n} e^{i2nt} = -i \frac{\Omega_R}{2} \delta_{n,0}, \end{aligned} \quad (22)$$

which implies the recursion relations

$$-i2nG_{2n} + D_0G_{2n} - D_2(G_{2n-2} + G_{2n+2}) = -i\frac{\Omega_R}{2}\delta_{n,0}. \quad (23)$$

Defining

$$R_{2n} = D_0 - i2n, \quad (24)$$

the equations for $n \geq 1$ give the continued fraction

$$G_2 = T_2 D_2 G_0, \quad (25)$$

with

$$T_2 = [R_2 - D_2[R_4 - D_2[R_6 - \dots]^{-1}D_2]^{-1}D_2]^{-1}. \quad (26)$$

The equations for $n \leq -1$ can be rearranged to get a similar relation that progresses towards negative n values,

$$D_2 G_{2n+2} = R_{2n} G_{2n} - D_2 G_{2n-2}, \quad n \leq -1, \quad (27)$$

which gives the continued fraction

$$G_{-2} = T_{-2} D_2 G_0, \quad (28)$$

with

$$T_{-2} = [R_{-2} - D_2[R_{-4} - D_2[R_{-6} - \dots]^{-1}D_2]^{-1}D_2]^{-1}, \quad (29)$$

and the solution of the recursion relations is

$$G_0 = -i \frac{\Omega_R}{2} [D_0 - D_2(T_2 + T_{-2})D_2]^{-1}, \quad (30)$$

from which the rest of the coefficients follow immediately using, e.g., Eq. (27).

For the excited level excitation probability we get the particular periodic solution taking the form

$$\sigma_{ee}(t) = \sum_n \frac{\Omega_R}{\Gamma^2 + (2n)^2} \text{Im} [G_{2n} (\Gamma - i2n) e^{i2nt}]. \quad (31)$$

When only the average over the period of the driven motion is relevant, it is the single $n = 0$ Floquet component that determines the result

$$\bar{\sigma}_{ee} = \frac{1}{T} \int_0^T \sigma_{ee}(t) dt = \frac{\Omega_R}{\Gamma} \text{Im} G_0, \quad (32)$$

with the rescaling of Eq. (16) implying that in the units used above,

$$T = 2\pi/\Omega = \pi. \quad (33)$$

In general, G_0 would still be given implicitly, requiring to solve the recursion relations, using Eq. (30). In the limit that the periodically-driven motion can be considered as frozen during the time-scale of the internal level dynamics, i.e. for

$$\Omega/2\pi \ll \Gamma/2, \quad (34)$$

the solution reduces to the known (low-saturation) Lorentzian probability of absorption of a photon [15], which can be obtained by setting $D_2 \rightarrow 0$ above,

$$\sigma_{ee}^0 = \frac{\Omega_R^2}{\Gamma^2 + (2\Delta_{\text{eff}})^2} = \frac{s/2}{1 + (2\Delta_{\text{eff}}/\Gamma)^2}. \quad (35)$$

Even if the condition in Eq. (34) does not hold, in the limit of small amplitude of the motion, the limit $D_2 \rightarrow 0$ can be taken and the expression in Eq. (35) can be linearized in the velocity and used, as discussed below.

III. MOTION IN A QUADRUPOLE TRAP WITH EXCESS MICROMOTION

We start with the z motion of an ion in a 1D time-dependent quadrupole potential, displaced by a constant electric field E_z ,

$$V_e = \frac{1}{2}(a_z - 2q_z \cos 2t)z^2 - E_z z. \quad (36)$$

The units are nondimensional, obtained by rescaling the time as in Eq. (16) by half the trap's driving frequency, $\Omega/2$, and rescaling the coordinate by a natural length-scale w (discussed below), absorbing also the ion charge e and mass m into the nondimensional parameters, a_z , q_z , and E_z in a standard way [10, 15, 22, 25], detailed also in App. A. The solution of the inhomogeneous linear Mathieu equation of motion (e.o.m) derived from V_e can be written as [24]

$$z(t) = \bar{z}(t) + u(t), \quad \bar{z} = \sum_n B_{2n} e^{i2nt}, \quad (37)$$

where $n \in \mathbb{Z}$ and $B_{2n} = B_{-2n}$. The term $\bar{z}(t)$, being π -periodic (since the rf drive frequency is 2 in rescaled units) is known as excess micromotion as it can (typically) be minimized, by using controlled electric fields (that make E_z effectively small). Although it cannot be cooled away [in contrast to $u(t)$], $\bar{z}(t)$ is completely coherent and not stochastic [17, 26], and in this work we assume that it is invariant under time-reversal. Equation (37) defines a time-dependent canonical transformation to the new coordinate $u(t)$, with the conjugate momentum

$$p = \dot{u}, \quad (38)$$

(with the mass equal to 1). The transformed Hamiltonian becomes

$$H_0(u, p, t) = \frac{1}{2}p^2 + V_{\text{M.o.}}(u, t), \quad (39)$$

with the nondimensional Mathieu oscillator potential

$$V_{\text{M.o.}}(u, t) = \frac{1}{2}(a_z - 2q_z \cos 2t)u^2. \quad (40)$$

We can now introduce the action-angle variables I and θ , defined by a second (time-dependent) canonical transformation, using two functions of the phase space and time,

$$I = \Lambda(u, p, t), \quad \theta = \Theta(u, p, t). \quad (41)$$

The action-angle variables constitute a very useful choice of variables, since I is conserved during the Hamiltonian motion in the time-dependent potential, in contrast to the energy. The exact transformation functions are given in App. C 1. To the leading order in q_z we can write

$$u \approx \sqrt{2I/\nu_z} \cos \theta, \quad (42)$$

$$p \approx -\sqrt{2I\nu_z} \sin \theta + q_z \sin(2t) \sqrt{2I/\nu_z} \cos \theta, \quad (43)$$

with

$$\theta(t) = \nu_z t + \phi, \quad (44)$$

where ϕ is determined by the initial conditions, and the characteristic exponent $\nu_z(a_z, q_z)$ of the Mathieu equation can be approximated by

$$\nu_z \approx \sqrt{a_z + q_z^2/2}, \quad a_z, q_z^2 \ll 1, \quad (45)$$

which determines the secular oscillation frequency in physical units,

$$\omega_z = \nu_z \Omega/2. \quad (46)$$

To the same accuracy we have for the coefficients of \bar{z} of Eq. (37),

$$B_0 \approx E_z/\nu_z, \quad B_2 \approx -B_0 q_z/4, \quad (47)$$

with the rest of the series truncated (App. C 1). We define the amplitude of excess micromotion to be the peak-to-peak oscillation due to E_z , given to this order by

$$A_z = 4B_2 = 2q_z E_z/\nu_z, \quad (48)$$

which is linear in E_z . At the same order we can approximate

$$\dot{\bar{z}}(t) = -\sum_{n>0} 4n B_{2n} \sin(2nt) \approx -A_z \sin(2t). \quad (49)$$

IV. LASER COOLING

A. Laser cooling in the finite lifetime treatment

In this subsection we review the semiclassical laser cooling framework developed in [15], as it is employed in this work in combination with the Floquet solution of the OBE presented in Sec. II B, and applied to the motion in a quadrupole trap as described in Sec. III. This approach is based on conservation of energy and momentum at each photon absorption event and each spontaneous emission occurring after a random delay due to the nonzero lifetime of the electronic excited level. Between the absorption and emission, we assume that the ion moves completely classically on an invariant torus of the Hamiltonian phase-space, and is decoupled from the electromagnetic field. The presented theory is valid in the limit of a low saturation of the transition [Eq. (13)], when the ion spends most of the time in its electronic ground-state, which is often chosen in practice for allowing to reach the lowest cooling limit.

For the 1D treatment presented in following, when the stochastic dynamics are slow in comparison with the Hamiltonian motion, integrating over the angle θ allows one to obtain an effective Fokker-Planck equation for the probability distribution $P(I, t)$

$$\frac{\partial P(I, t)}{\partial t} = -\frac{\partial S(I, t)}{\partial I} \equiv -\frac{\partial}{\partial I} [\Pi_I P] + \frac{1}{2} \frac{\partial^2}{\partial I^2} [\Pi_{II} P], \quad (50)$$

with S the probability flux. Denoting with an overbar the torus average over any function $\Xi[I, \theta, t]$ of the phase space which is assumed to have some arbitrary period T ;

$$\Xi[I, \theta, t + T] = \Xi[I, \theta, t], \quad (51)$$

we define

$$\bar{\Xi}(I) \equiv \frac{1}{T} \int_0^T dt \frac{1}{2\pi} \int \Xi[I, \theta, t] d\theta. \quad (52)$$

The action drift and diffusion coefficients, respectively, entering Eq. (50) for the laser cooling setup considered here are

$$\Pi_I(I) = \Gamma\rho \left[p_r \frac{\partial \Lambda}{\partial p} + \frac{1}{2} p_r^2 \left(\frac{\partial^2 \Lambda}{\partial p^2} + \mu \left\langle \frac{\partial^2 \Lambda}{\partial p^2} \right\rangle_{\Gamma} \right) \right], \quad (53)$$

$$\Pi_{II}(I) = \Gamma\rho \left[p_r^2 \left(\frac{\partial \Lambda}{\partial p} \right)^2 + p_r^2 \mu \left\langle \left(\frac{\partial \Lambda}{\partial p} \right)^2 \right\rangle_{\Gamma} \right], \quad (54)$$

where μ is a constant of order unity [15], which stems from the second moment of the dipole radiation pattern (and is often denoted by α [5] or ξ [10] in the existing literature), and $p_r = \hbar k$ is the photon recoil momentum with \hbar rescaled as in Eq. (A4). The other terms in the right hand side of Eqs. (53)-(54) are all functions of the phase space time and point where a photon absorption occurred,

$$Z_a \equiv \{u, p, t\}, \quad (55)$$

that is averaged on a given torus by the definition in Eq. (52). The required derivatives of the action-angle transformation function $\Lambda(u, p, t)$ [defined in Eq. (41)], can be found in App. A, and to the leading order in q_z [Eq. (45)], coincide with the simple formulae for the harmonic oscillator,

$$\frac{\partial \Lambda}{\partial p} \approx -\sqrt{2I/\nu_z} \sin \theta, \quad \frac{\partial^2 \Lambda}{\partial p^2} \approx \frac{1}{\nu_z}. \quad (56)$$

We stress that the approximation in Eq. (56) gives accurate results for the excess micromotion (with a neglected contribution approximately equal to $q_z^2/4$).

The rate of photon absorption-emission cycles in the low-saturation limit as a function of the phase-space point is given by $\Gamma\rho$, where in general one should take $\rho = \sigma_{ee}(t)$, the excited level population defined in Sec. II. The different limits of $\sigma_{ee}(t)$ employed in this work are discussed in Sec. IV B. The emission phase space point is averaged over through the integration of the waiting time distribution $\langle \cdot \rangle_{\Gamma}$. Given an absorption that occurred at the phase-space point Z_a , the mean value of any function of the phase space, at the time of emission, is given by

$$\langle \Xi(Z_a) \rangle_{\Gamma} \equiv \int_0^{\infty} \Gamma e^{-\Gamma t'} \Xi(Z(t+t'); Z(t) = Z_a) dt'. \quad (57)$$

The time integral in Eq. (57) is to be performed along the trajectory, denoted with the notation of Eq. (55) as $Z(t+t')$, as it starts at the phase space point Z_a and evolves according to the Hamiltonian motion at fixed I . The zero lifetime limit can be obtained from the treatment above

if in Eq. (57) it can be assumed [15] that $\Gamma e^{-\Gamma t'} \approx \delta(t')$. In addition, an adiabaticity condition is assumed that justifies the averaging of Eq. (52). A simple criterion is obtained by requiring a small relative change in action due to both drift and diffusion, during a cycle of the motion:

$$\Pi_I/\nu_z \ll I, \quad \Pi_{II}/\nu_z \ll I^2. \quad (58)$$

A steady-state of the FP equation with appropriate boundary conditions can be obtained by setting the left-hand-side to 0, and then noting that the reflecting boundary condition at the origin [$S(I=0, t) = 0$] implies that this would be a zero-current state [$S(I, t) = 0$]. Integrating the resulting equation gives the time-independent distribution

$$P(I) = \mathcal{N} [\Pi_{II}(I)]^{-1} \exp \left\{ 2 \int^I \frac{\Pi_I(I')}{\Pi_{II}(I')} dI' \right\}, \quad (59)$$

with \mathcal{N} the normalization factor. This steady-state solution is relevant if the exponential decays fast enough (as a function of I), implying physically that indeed the ion remains trapped for a long time in a bounded region of phase space.

B. The photon absorption probability

Using the steady-state distribution $P(I)$ of Eq. (59) we can define the mean value of any function of the phase-space (averaged over the angles), e.g. the mean action

$$\langle I \rangle \equiv \int_0^{\infty} I P(I) dI, \quad (60)$$

which, using Eq. (3) that neglects the zero-point motion, gives immediately the mean phonon number

$$\langle n \rangle \equiv \int_0^{\infty} I P(I) dI / \hbar. \quad (61)$$

The mean photon scattering rate is also important, and in particular it can be measured experimentally,

$$\langle R \rangle \equiv \int_0^{\infty} \bar{\Gamma} \rho P(I) dI. \quad (62)$$

Finally, we are left with the need to specify the photon absorption probability function ρ . For the 1D dynamics studied here, the effective detuning due to the Doppler shift is

$$\Delta_{\text{eff}} = \Delta - k v_z(p, t), \quad (63)$$

with k being the 1D laser wavenumber, and the real-space velocity $v_z(p, t)$ that is a function of the canonical

momentum $p(t)$ expanded about $\bar{z}(t)$ and the time t , is given [using Eq. (37)] by

$$v_z = \dot{z}(t) = \dot{\bar{z}}(t) + p(t). \quad (64)$$

To leading order in q_z , using Eqs. (43)-(44) and Eq. (49), and under the assumption that $\nu_z/2\pi \ll \Gamma/2$ which allows to treat θ as frozen on the time-scale leading to a stationary state in the internal dynamics, we see that Eq. (63) can be plugged in Eq. (21) with the expansion coefficients

$$D_0 = -i(\Delta + k\sqrt{2I\nu_z} \sin \theta) - \Gamma/2, \quad (65)$$

$$D_2 = -ik(A_z - q_z\sqrt{2I/\nu_z} \cos \theta)/2. \quad (66)$$

Thus, for the most general case (in the low-saturation limit) we should plug $\rho = \sigma_{ee}(t)$ of Eq. (31) in Eqs. (53)-(54). With the approximation of Eq. (56), none of the other terms (except ρ) in Eqs. (53)-(54) depend on t , and hence the average over a micromotion period in Eq. (52) can be carried out independently as in Eq. (32), resulting in the simpler expression

$$\rho = \bar{\sigma}_{ee}(p). \quad (67)$$

In the limit $D_2 \rightarrow 0$, we can use Eq. (35);

$$\rho \rightarrow \sigma_{ee}^0(v_z). \quad (68)$$

This limit can be taken when both the excess micromotion amplitude and the action are low enough (the cooling limit without excess micromotion, treated analytically in Sec. IV C), and when the micromotion frequency is low enough, when the condition of Eq. (34) holds.

C. The cooling limit without excess micromotion

In this subsection we summarize the results of a derivation of the Doppelp cooling limit presented in detail for the general 3D motion as in App. B. In the absence of excess micromotion, the ion velocities can be assumed to be small near the origin of the quadrupole trap. This defines a specific limit of the cooling, that can in fact be analyzed analytically. In this limit the Lorentzian $\rho = \sigma_{ee}^0$ of Eq. (35) can be used as discussed above, and can be linearized in the velocity, subject to the condition

$$I \ll I_{\text{linear}} = \left(\frac{\Gamma^2 + 4\Delta^2}{8k\Delta} \right)^2 \frac{1}{2\nu_z}. \quad (69)$$

In this approximation, we can write for the action drift and diffusion coefficients (with $s \ll 1$), using the expressions given in App. B and using Eq. (A16),

$$\Pi_I^l = \gamma I + \frac{1}{2}i_z, \quad \Pi_{II}^l = i_z I, \quad (70)$$

with

$$i_z = p_r F_r (1 + \mu) c_z, \quad (71)$$

where the mean radiation force and the rate of momentum damping having the well-known forms ([3, 10, 15], respectively,

$$F_r = \frac{p_r \Gamma s/2}{1 + (2\Delta/\Gamma)^2}, \quad \gamma = \frac{4kp_r s \Delta/\Gamma}{[1 + (2\Delta/\Gamma)^2]^2}, \quad (72)$$

i_z generalizes a similar coefficient for the harmonic oscillator [15], and c_z is defined in Eq. (C14), while to the leading order in q_z , using Eqs. (45) and (56), we have

$$c_z \approx \nu_z^{-1}. \quad (73)$$

Then for $\Delta < 0$ the final stage of the cooling reduces to an exponential, thermal equilibrium-like distribution in the conserved action, that is nearly identical to the well-known Doppler cooling limit that is obtained in limit of a vanishing excited level lifetime within a static harmonic potential (the heavy particle [3]). The equilibrium is determined by the balance of momentum dissipation and diffusive heating. It is a zero-current distribution in the action, given by

$$P(I) = \lambda_z e^{-\lambda_z I}, \quad (74)$$

where $\lambda_z = -2\gamma/i_z$, which gives the mean and standard deviation of the action, $\langle I \rangle = \sqrt{\langle (I - \langle I \rangle)^2 \rangle} = \lambda_z^{-1}$, can be obtained from Eq. (B24) and reads here

$$I_{\text{limit}} \equiv \lambda_z^{-1} = \hbar \frac{\Gamma}{8} c_z (1 + \mu) \left[\frac{\Gamma}{2|\Delta|} + \frac{2|\Delta|}{\Gamma} \right]. \quad (75)$$

Although the standard Doppler cooling limit [10] is derived by assuming an ion in a time-independent potential and being stationary in space during a photon absorption-emission cycle, the final distribution derived here, for motion with micromotion, turns out to be thermal as well, and coincides with that of the harmonic oscillator of the same secular frequency, up to the correction due to c_z not being exactly $1/\nu_z$. These results have been found numerically in the example studied in [15], and here it is derived for the general case. The fact that the ion can emit the photon at a random time along the trajectory after the absorption, and hence with the ion's a momentum (or kinetic energy) being very different than that at the absorption, does not lead on average to an increase in the action diffusion due to the scattering events. The analysis in App. B indicates that this is a consequence of the memoryless decay process together with the linearity of the oscillations, and the linearity of the Lorentzian (in the small velocity limit). Under such conditions, the phase-space averaging of such scattering events (with the accessible ion momenta), cancels out the effects of micromotion (to leading order). It serves to show the strength of the action-angle as the right choice of coordinates for analyzing the motion in the time-dependent potential.

D. Optimal cooling with excess micromotion

In this subsection we consider the optimal choice of detuning for cooling the ion to the narrowest (exponential) distribution in action, in the 1D setting. Assuming that an exponential distribution can indeed be obtained (as shown using the numerical calculations presented in Sec. I and Sec. V), it can be characterized as just by using the observable photon scattering rate. The following derivation does not assume a specific form for the photon absorption probability, only that it is a function of the Doppler shift defined in Eq. (15), i.e.

$$\rho = \rho(\Delta_{\text{eff}}) = \rho(\Delta - k\dot{z} - kp). \quad (76)$$

In the following we will refer to the two partial derivatives

$$\partial_{\Delta}\rho = \rho'(\Delta_{\text{eff}}), \quad \partial_p\rho = -k\rho'(\Delta_{\text{eff}}), \quad (77)$$

where ρ' denotes the derivative with respect to the argument. Defining the Doppler shift at $p = 0$, due only to excess micromotion,

$$\Delta_e(t) = \Delta - k\dot{z}(t), \quad (78)$$

we can Taylor expand the Lorentzian in the momentum,

$$p_r\Gamma\rho \approx F_e(t) + \gamma_e(t)p, \quad (79)$$

with

$$F_e(t) = p_r\Gamma\rho[\Delta_e(t)], \quad \gamma_e(t) = -p_r\Gamma k\rho'[\Delta_e(t)]. \quad (80)$$

Let us assume that $F_e(t)$ and $\gamma_e(t)$ can be averaged in time independently of the torus averaging and of the spontaneous emission waiting time. This can be justified in the small amplitude limit as in App. B. We define

$$\bar{F}_e = \frac{1}{\pi} \int_0^\pi F_e(t) dt, \quad \bar{\gamma}_e = \frac{1}{\pi} \int_0^\pi \gamma_e(t) dt. \quad (81)$$

Then the resulting distribution will take again an exponential form

$$P(I) = \lambda_e e^{-\lambda_e I}, \quad \lambda_e = -2\bar{\gamma}_e/h_e \quad (82)$$

where

$$h_e = p_r\bar{F}_e(1 + \mu)c_z. \quad (83)$$

The mean final action is $\langle I \rangle = \lambda_e^{-1}$. We now show that it can be deduced by simply measuring the photon scattering rate. Using the expansion of Eq. (79) we can write for the torus average defined in Eq. (52)

$$\bar{\Gamma}\rho \approx \frac{1}{p_r} \overline{(F_e(t) + \gamma_e(t)p)} = \bar{F}_e/p_r, \quad (84)$$

since Eq. (43) implies that $\bar{p} = 0$. We therefore have using Eq. (62),

$$\langle R \rangle \approx \int dIP(I)\bar{F}_e/p_r = \bar{F}_e/p_r, \quad (85)$$

and also

$$\partial_{\Delta}\langle R \rangle \approx \partial_{\Delta}\bar{F}_e/p_r = \overline{\Gamma\rho'[\Delta_e(t)]} = -\bar{\gamma}_e/(p_r k). \quad (86)$$

Hence we can derive the very useful relation

$$\langle I \rangle = \lambda_e^{-1} \approx \frac{1}{2}\hbar(1 + \mu)\nu_z^{-1} [\partial_{\Delta}\ln\langle R \rangle]^{-1}. \quad (87)$$

Using Eq. (87) we can deduce that the optimal detuning curve $\Delta_{\text{optimal}}(A_z)$ can be found simply by looking for a maximum of the experimental observable $\partial_{\Delta}\ln\langle R \rangle$, and the mean action or phonon number of the resulting thermal distribution can be deduced, and in particular we obtain immediately Eq. (4) with the proportionality constant

$$\tilde{n} = \frac{1}{2}(1 + \mu)\nu_z^{-1}. \quad (88)$$

V. THERMAL AND NONTHERMAL DISTRIBUTIONS IN THE FINAL STAGE

For the numerical calculations presented in this section we fix the Mathieu parameters for the z motion,

$$a_z = -0.0002, \quad q_z \approx 0.16, \quad (89)$$

and the Floquet characteristic exponent is

$$\nu_z \approx 0.1126. \quad (90)$$

In the following subsections we consider the cases of the micromotion frequency being either low or high with respect to (half) the excited level linewidth, whereas the intermediate regime has been laid down in Sec. I.

A. The cooling limit with low-frequency excess micromotion

In this subsection we take a $^{24}\text{Mg}^+$ ion. The dimensional laser parameters that we consider are

$$\tilde{k} \approx 2\pi/280 \text{ nm}^{-1}, \quad \tilde{\Gamma} \approx 263 \times 10^6 \text{ s}^{-1}, \quad (91)$$

and the spontaneous emission coefficient is

$$\mu = 2/5. \quad (92)$$

The micromotion frequency taken here is

$$\Omega = 2\pi \times 20 \text{ MHz}, \quad (93)$$

and the resulting secular frequency [Eq. (46)] is

$$\omega_z \approx 2\pi \times 1.1 \text{ MHz}. \quad (94)$$

The condition of Eq. (34) is (approximately) obeyed, and hence we are in this subsection approaching the limit of

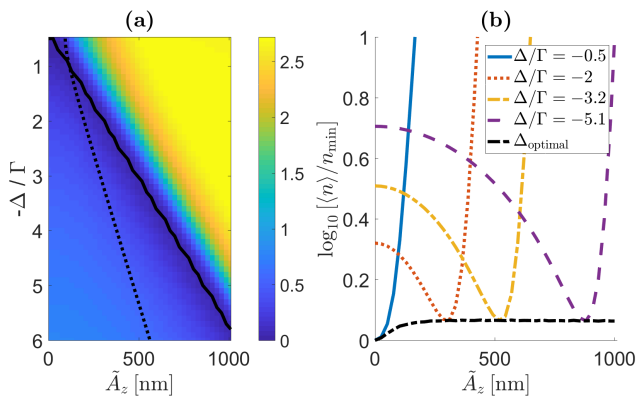


FIG. 4. (a) The mean final phonon number $\langle n \rangle$ [Eq. (61)] as a function of the detuning and the excess micromotion amplitude as in Fig. 1 with the parameters of Eqs. (89)-(93). This figure presents a calculation in the limit of low micromotion frequency, for which the photon absorption probability is taken to be the Lorentzian $\rho = \sigma_{ee}^0$ of Eq. (35), assuming that the micromotion dynamics are frozen on the scale of the excited level dynamics. For $A_z \ll A_{\text{linear}}(\Delta)$ [shown as the dotted curve and defined in Eq. (97)], the effect of the excess micromotion can be neglected. The solid black curve gives a simplified approximation [Sec. V A] for the optimal detuning curve $\Delta_{\text{optimal}}(A_z)$ for which $\langle n \rangle$ can be reduced to a minimum. (b) Curves obtained from the map of panel (a), showing the attainable minima of the action as a function of the excess micromotion amplitude. Here the vertical axis is truncated at 1, corresponding to $\langle n \rangle = 10 \times n_{\text{min}}$. See the text for a discussion of the nonmonotonic features of these curves, and compare with Fig. 5.

a micromotion frequency much smaller than (half) the excited level decay rate.

Figure 4 shows the mean phonon number $\langle n \rangle(A_z, \Delta)$ in the steady state of cooling as a function of the excess micromotion and the detuning, obtained by calculating the action distribution and using the approximate semiclassical relation Eq. (3), as in Eq. (61). We here employ for the photon absorption probability the Lorentzian $\rho = \sigma_{ee}^0$ of Eq. (35) and substitute the velocity v_z of Eq. (64), which includes the excess micromotion, approximated as being frozen during the timescale of the internal level dynamics. In the figure we use the dimensional variable

$$\tilde{A}_z = wA_z, \quad (95)$$

given in nanometers. With $w = 100 \mu\text{m}$, \tilde{A}_z extends to 10^{-2} in this figure, which corresponds to $A_z = 1000$ nm, obtained for $E_z = 80$ V/m.

We define the minimal mean action that is obtained in the upper left corner of the figure,

$$I_{\text{min}} \equiv \langle I \rangle(A_z = 0, \Delta = -\Gamma/2), \quad (96)$$

and using Eq. (75), we have to an accuracy of order $q_z^2/4$, $I_{\text{min}} = I_{\text{limit}}(\Delta = \Gamma/2)$. For increased values of A_z (with

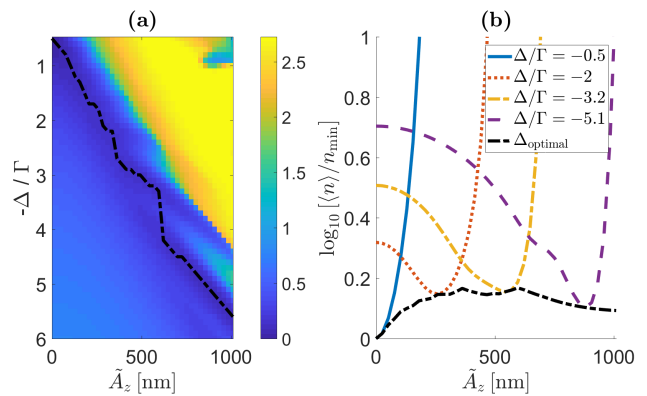


FIG. 5. As Fig. 4, but rather calculated using the Floquet-approach photon absorption probability $\rho = \bar{\sigma}_{ee}$ of Eq. (32), which accounts more accurately for the periodically-driven excess micromotion oscillation. The dashed-dotted black curve denotes the optimal detuning curve $\Delta_{\text{optimal}}(A_z)$. In comparison with Fig. 4, some deviations are seen to result from narrow Floquet tongues, which are similar (but thinner than) those apparent in Fig. 1 where the micromotion frequency is higher and comparable to the internal decay rate.

$\Delta = -\Gamma/2$ fixed), the value of $\langle I \rangle$ grows slowly at first and then rises sharply, and the distribution becomes non-thermal (as will be discussed in the following). We show [App. C 2] that indeed the linear term in the expansion of $\langle I \rangle$ as a function of A_z (at any fixed Δ) vanishes [for the model of Eq. (36), with a static stray electric field]. In the region $A_z \ll A_{\text{linear}}(\Delta)$ defined by

$$A_{\text{linear}}(\Delta) = [\Gamma^2 + 4\Delta^2] / (8k|\Delta|), \quad (97)$$

the effect of the micromotion is small, and $\langle I \rangle$ grows approximately inversely as a function of Δ . This curve, $A_{\text{linear}}(\Delta)$, is indicated by a dotted line in Fig. 4(a).

For detunings $\Delta \lesssim -0.8\Gamma$, we find that $\langle I \rangle$ first decreases with A_z , reaching a minimal value before growing sharply. This is a result of the coefficient at order $(A_z)^2$ in the expansion of $\langle I \rangle$ being negative in that region, as shown in App. C 2. Using the analytic form of ρ we can obtain the function $\Delta_{\text{optimal}}(A_z)$, by expanding the Lorentzian in p [see App. IV D] and maintaining the periodic excess micromotion part,

$$p_r \Gamma \rho \approx F_e(t) + \gamma_e(t)p, \quad (98)$$

with $F_e(t)$ and $\gamma_e(t)$ defined in Eq. (80) taking the explicit form

$$F_e(t) = \frac{p_r \Gamma s / 2}{1 + (2\Delta_e(t)/\Gamma)^2}, \quad \gamma_e(t) = \frac{4k p_r s \Delta_e(t) / \Gamma}{[1 + (2\Delta_e(t)/\Gamma)^2]^2}, \quad (99)$$

and $\Delta_e(t)$ is defined in Eq. (78). In the absence of micromotion, the above expansion reduces to the coefficients in Eq. (72). The coefficients in Eq. (99) can be explicitly integrating using \dot{z} of Eq. (37) approximated as in Eq. (49)

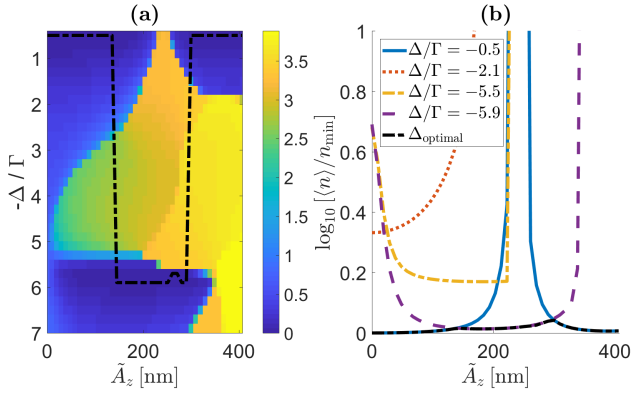


FIG. 6. As in Fig. 5, however for a ${}^9\text{Be}^+$ ion, with trap and micromotion parameters given in Eqs. (100)-(102), approaching the limit of a high micromotion frequency. The effect of a single Floquet resonance is clearly seen, emanating from the parametric Floquet resonance at $\Delta = -\Omega$ (the micromotion sideband), i.e. $-\Delta/\Gamma \approx 5.3$, with a steeper dependence of the phonon distribution mean on the parameters [see panel (b)].

to obtain \bar{F}_e and $\bar{\gamma}_e(t)$ of Eq. (81) and the explicit form of the action distribution along $\Delta_{\text{optimal}}(A_z)$ found from minimizing the resulting mean action. $\Delta_{\text{optimal}}(A_z)$ calculated in that way can be seen to be a nearly straight line (curving only close to $\Delta = -\Gamma/2$) depicted by the solid black curve in Fig. 4(a), and the final action depends only weakly on A_z . The more accurate calculation based on the Floquet-approach photon absorption probability $\rho = \bar{\sigma}_{ee}$ of Eq. (32), which accounts explicitly for the periodically-driven excess micromotion, is presented in Fig. 5, with some small but noticeable deviations (more so in the large detuning and \tilde{A}_z regime). The Floquet corrections decrease in the limit of $\Omega/2\pi \ll \Gamma/2$.

B. The cooling limit with high-frequency excess micromotion

Figures 1-3 of Sec. I present the analysis of the cooling with a ${}^{24}\text{Mg}^+$ ion but with a micromotion frequency which is 2.5 times larger than that taken in Fig. 5. As discussed briefly in Sec. I, the noticeable Floquet “tongues” seen Fig. 1 can be attributed to Floquet (parametric) resonances (see also App. D)). A more extensive treatment of these Floquet resonances is beyond the scope of the current work. However, in order to approach the limit of a high micromotion frequency with respect to the linewidth, we consider here also the example of a ${}^9\text{Be}^+$ ion, with

$$\tilde{k} \approx 2\pi/313 \text{ nm}^{-1}, \quad \tilde{\Gamma} \approx 120 \times 10^6 \text{ s}^{-1}, \quad (100)$$

$\mu = 2/5$ as in Eq. (92) and the micromotion frequency

$$\Omega = 2\pi \times 100 \text{ MHz}, \quad (101)$$

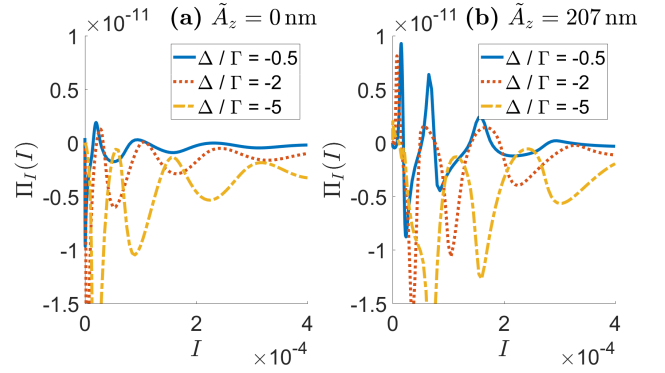


FIG. 7. The action drift coefficient $\Pi_I(I)$ of Eq. (53) as a function of the nondimensional action I , for parameters as in Fig. 6 (with a high micromotion frequency) and using the length scale of Eq. (103). (a) For $\Delta = -\Gamma/2$ and in the absence of excess micromotion, $\Pi_I(I)$ crosses 0 with a negative slope at two high action values, which become possible metastable points of the cooling where the ion may get captured above the steady state at the Doppler cooling limit. (b) For a large value of excess micromotion amplitude the number of such metastable zero crossings may increase, together with the width of the region where $\Pi_I(I) > 0$ (which forms an effective barrier for the diffusion of the ion to the low action states). The I axis extends here to motion (expanded about the excess micromotion) with an amplitude $\tilde{u} \sim 4\mu\text{m}$, and beyond the presented range the oscillations in $\Pi_I(I)$ decay and we find the asymptotic scaling $\Pi_I(I) \propto -1/\sqrt{I}$ [15].

which gives using the same Mathieu parameters as in above, the secular frequency

$$\omega_z \approx 2\pi \times 5.6 \text{ MHz}. \quad (102)$$

Figure 6 shows the structure induced by a single dominant Floquet tongue that emerges from $\Delta = -\Omega$, i.e. $-\Delta/\Gamma \approx 5.3$. Passing this resonance corresponds to cooling on a micromotion sideband, which, as seen, can be advantageous in a range of \tilde{A}_z values.

Finally, the mean steady state phonon number (or action) is not the only interesting quantity when studying laser cooling. For example, the time required to cool down from a high amplitude motion, and the probability for the ion to be lost from the trap in the process due to diffusion, are just two examples of dynamics of the cooling process that are very interesting and can be calculated. The latter question has been treated in some detail in [15], and the former requires a detailed study of the FP dynamics. One important feature of the cooling dynamics in that case is presented in Fig. 7. For comparison with the calculations presented in [15] we take the distance scaling unit

$$w = 50 \mu\text{m}, \quad (103)$$

and present the action drift coefficient $\Pi_I(I)$ of Eq. (53) in terms of the nondimensional action I . It can be seen

that for this high micromotion frequency, even without excess micromotion, there are for $\Delta = -\Gamma/2$ two high action values where $\Pi_I(I)$ crosses 0 with a negative slope, which is a possible metastable point of the cooling where the ion may get captured en route to being cooled to steady state at the Doppler cooling limit. The asymptotics of the drift coefficient beyond the presented range converges to $\Pi_I(I) \propto -1/\sqrt{I}$ as discussed in [15]. For large excess micromotion the number of such metastable zero crossings may increase, together with the width of the region where $\Pi_I(I) > 0$ (which forms an effective barrier for the diffusion of the ion to the low action states). For larger detunings the opposite trend is seen, with the peaks wherein $\Pi_I(I) > 0$ decreasing, leading to an expected more efficient and faster cooling of the ion, strengthening the conclusion of [15]; superimposing a laser with a larger detuning in traps operated at high micromotion frequency is advantageous for keeping the ion trapped and preventing it from being stuck in intermediate metastable states of motion.

VI. SUMMARY AND OUTLOOK

The main result of the current work has two aspects. On the practical side, our main result is that excess micromotion of a large amplitude does not prevent reaching a low, thermal-like distribution for the fluctuations expanded about the coherent driven motion, achievable by simply tuning the cooling laser frequency. This is useful in particular when considered in the context of ion crystals discussed below. This concrete result also demonstrates a broad conclusion that can be drawn, which is that even though the ion is strongly driven by the trap potential in combination with the stochastic photon scattering processes, by choosing the right frame, the driven and the stochastic dynamics can be separated, with each becoming considerably simpler. The action-angle coordinates form the right coordinates because the fluctuations in action represent the relevant stochastic, noncoherent part of the motion, and moreover the angles can be safely coarse grained, leaving a clear picture of the underlying complex dynamics in terms of the actions.

An important foreseeable application of the presented results is to a crystal of ions. In a crystal configuration for which some ions are not positioned at a point where the rf potential vanishes (e.g. in a planar configuration in a linear Paul trap), those ions will perform driven periodic motion akin to excess micromotion, determined by the interplay of the Coulomb interaction and the periodic drive [22]. It is the dynamic equivalent of an ion's equilibrium position in a static crystal, and cannot be removed. By tailoring the laser detuning, the final action distribution of these ions can be significantly reduced. A setup consisting of a few lasers can be treated by adding the

drift and diffusion coefficients calculated separately for each laser. Spatially inhomogeneous laser profiles and laser parameters which are modulated in time can be transparently treated. In combination with noise heating [15], a detailed characterization of the final distribution of laser-cooled ions and the dynamics leading to it can be obtained, and ideas for its manipulation can be explored [27]. The ensuing dynamics can be studied using the analytic tools of App. A, by expansion in small linearized deviations about the driven periodic motion. This way, cooling and heating dynamics corresponding to Gaussian white noise, and the stationary distribution of chains of ions in 1D and crystals in 2D and 3D configurations, can be studied [28–43]. The theory of Ornstein–Uhlenbeck processes can be applied for a detailed analysis and at the same time be tested experimentally in a controlled way [44].

Interesting extensions of the theory could include more general electronic level structures [14, 45], and applying the action-angle framework to setups where power-law distributions in energy (in an averaged sense) were predicted for collisions of ions with neutral atoms [46–49]. The interplay of micromotion, noise and laser cooling is of significant importance for applications in quantum information processing and the operation of quantum gates and entanglement operations with trapped ions [19, 22, 26, 50–64]. In particular, as discussed above, the actions standing at the heart of the current work correspond exactly to the quantum mechanical phonons with a periodically-driven harmonic potential [65], in terms of Floquet-Lyapunov modes [22, 24]. Using the exact time-dependent wavefunctions in quadrupole traps [24, 66], would allow to extend the theory to the quantum limit.

ACKNOWLEDGMENTS

H.L. thanks Ananyo Maitra, Dietrich Leibfried, Denis Ullmo, and Roni Geffen for fruitful discussions, and acknowledges support by IRS-IQUPS of Université Paris-Saclay, and by LabEx PALM under grant number ANR-10-LABX-0039-PALM.

Appendix A: A coupled system of Mathieu oscillators

We consider an ion that has been cooled to the center of a Paul trap of a general type. We assume that the potential can be approximated as a quadrupole (this is however not necessarily the case in multipole traps [67]). With \vec{r} and $\vec{v} \equiv \dot{\vec{r}}$ being the vector coordinate and velocity of an ion in $D = 3$ dimensions, we first rescale the time t by half the micromotion frequency, and the coordinates by a natural unit of length, w , relevant for the

trap at hand,

$$\vec{r} \rightarrow \vec{r}/w, \quad t \rightarrow \Omega t/2, \quad \vec{v} \rightarrow \vec{v}/(w\Omega/2). \quad (\text{A1})$$

Using the rescaling in Eq. (A1) allows us also to define a nondimensional momentum using the ion mass m and by absorbing it and the ion charge e into the parameters, we define a nondimensional potential energy V resulting from an electrostatic voltage U ,

$$V \rightarrow V/[mw^2\Omega^2/(4e)], \quad (\text{A2})$$

a nondimensional electric field,

$$E \rightarrow E/[mw\Omega^2/(4e)], \quad (\text{A3})$$

and a nondimensional Planck constant scaled according to

$$\hbar \rightarrow \hbar/(mw^2\Omega/2). \quad (\text{A4})$$

In general, the quadrupole potential may be composed of a sum of a few quadrupole potential terms whose origin does not coincide, or there may be ‘‘stray’’ electric fields that push the ion from the origin of the quadrupole potential. The resulting motion contains a component known as ‘‘excess micromotion’’, since it can (typically) be minimized by using additional DC electric fields. In this case it is useful to describe the motion by using generalized coordinates \vec{u} with conjugate momenta \vec{p} , differing from the real space position \vec{r} and velocity \vec{v} (with $m = 1$) by a time-dependent displacement [22], that eliminates the terms linear in the coordinates from the potential energy,

$$\vec{r}(t) = \vec{r}^0(t) + \vec{u}(t), \quad \vec{v}(t) = \dot{\vec{r}}^0(t) + \dot{\vec{p}}(t). \quad (\text{A5})$$

We assume that the nondimensional potential $V(\vec{u}, t) = V(\vec{u}, t + \pi)$ is time-reversal invariant and π -periodic (which can include the particular case where it is time-independent), and can be expanded into a system of D coupled Mathieu oscillators [22], obtaining the nondimensional Hamiltonian

$$H_0(\vec{u}, \vec{p}, t) = \frac{1}{2}(\vec{p})^2 + V_{\text{M.o.}}(\vec{u}, t), \quad (\text{A6})$$

with

$$V_{\text{M.o.}}(\vec{u}, t) = \frac{1}{2}\vec{u}^t (A - 2Q \cos 2t) \vec{u} \quad (\text{A7})$$

where \vec{u}^t denotes the transpose, and A, Q are matrices that describe the linearized DC and rf voltages tensors. By the Laplace equation, $\text{tr}A = \text{tr}Q = 0$. The equations of motion derived from the linearized potential form a coupled system of parametric oscillators [24, 68]. If A and Q commute, then they can be diagonalized to give a system of decoupled Mathieu equations. In the opposite

case, no such simple transformation exists, and the three spatial directions will be mixed by the micromotion.

The most general solution of this motion is a sum over D decoupled linear oscillators

$$\vec{u} = \sum_j \sqrt{I_j} \left(2\text{Re} \sum_n \vec{C}_{2n}^j e^{i2nt} e^{i\theta_j} \right), \quad (\text{A8})$$

$$\vec{p} = - \sum_j \sqrt{I_j} \left(2\text{Im} \sum_n \vec{C}_{2n}^j (2n + \nu_j) e^{i2nt} e^{i\theta_j} \right), \quad (\text{A9})$$

where the n summation extends over \mathbb{Z} and the coefficients \vec{C}_{2n}^j for $n \neq 0$ give the micromotion modulation. In Eqs. (A8)-(A9) we have defined

$$\theta_j = \nu_j t + \phi_j, \quad (\text{A10})$$

with ν_j the characteristic exponents of the Mathieu system, that are related to the secular frequencies of motion in the trap (ω_j , in physical units), by

$$\omega_j = \nu_j \Omega/2, \quad (\text{A11})$$

and I_j and ϕ_j are (for now) arbitrary constants related to the initial conditions. We assume that the motion is stable, i.e. that ν_j are all real, and are between 0 and 1.

As detailed in [24], a time-dependent (Floquet-Lyapunov) linear transformation can be used to transform the real space coordinates and momenta, to new (complexified) coordinates $\vec{\xi}$ and the canonically conjugate momenta $-i\vec{\chi}$,

$$\begin{pmatrix} \vec{u} \\ \vec{p} \end{pmatrix} = \Gamma(t) \begin{pmatrix} \vec{\xi} \\ \vec{\chi} \end{pmatrix}, \quad \Gamma(t) = \begin{pmatrix} U & U^* \\ V & V^* \end{pmatrix} \quad (\text{A12})$$

where $U(t), V(t)$ are $D \times D$ complex matrices constructed from the π -periodic part of the D column vector solutions given in Eqs. (A8)-(A9), i.e.

$$U = \left(\sum \vec{C}_{2n}^j e^{i2nt} \dots \right), \quad V = \left(i \sum (2n + \nu_j) \vec{C}_{2n}^j e^{i2nt} \dots \right), \quad (\text{A13})$$

and U^* is the complex conjugate matrix, and we will use U^\dagger for the hermitian conjugate matrix, and also U^t that is the transposed matrix. These matrices are to be rescaled by multiplication by a constant diagonal matrix,

$$U \rightarrow U(-2iV^t(0)U(0))^{-1/2}, \quad (\text{A14})$$

and V similarly, guaranteeing the normalization

$$V^t(0)U(0) = \frac{1}{2}i, \quad (\text{A15})$$

which also implies the identity (that will be used later),

$$U^t(t)V^*(t) - V^t(t)U^*(t) = -i. \quad (\text{A16})$$

Then the transformation in Eq. (A12) is canonical and its inverse is

$$\begin{pmatrix} \vec{\xi} \\ \vec{\chi} \end{pmatrix} = \Gamma^{-1}(t) \begin{pmatrix} \vec{u} \\ \vec{p} \end{pmatrix}, \quad \Gamma^{-1}(t) = \begin{pmatrix} iV^\dagger & -iU^\dagger \\ -iV^t & iU^t \end{pmatrix}. \quad (\text{A17})$$

The Hamiltonian then transforms according to

$$H_0(\vec{\xi}, \vec{\chi}) = \frac{1}{2} \sum_j \nu_j (\xi_j \chi_j + \chi_j \xi_j). \quad (\text{A18})$$

The time evolution of the new canonical coordinates is given by (noting that $\xi_j = \chi_j^*$)

$$\xi_j(t) = \sqrt{I_j} e^{i(\nu_j t + \phi_j)}, \quad \chi_j(t) = \sqrt{I_j} e^{-i(\nu_j t + \phi_j)}. \quad (\text{A19})$$

We can now introduce naturally a second canonical transformation to the action-angle coordinates $(\vec{I}, \vec{\theta})$,

$$I_j = \xi_j \chi_j, \quad \theta_j = i \ln \chi_j, \quad (\text{A20})$$

which justifies the notation in Eq. (A10), since

$$\xi_j = \sqrt{I_j} e^{i\theta_j}, \quad \chi_j = \sqrt{I_j} e^{-i\theta_j}, \quad (\text{A21})$$

whence the Hamiltonian obtains the simple form

$$H_0(\vec{I}) = \sum_j \nu_j I_j. \quad (\text{A22})$$

Since this is the canonical Hamiltonian of simple decoupled harmonic oscillators, the quantum levels can be obtained by using the well-known relation semiclassical quantization relation [69],

$$n_j + 1/2 = I_j/\hbar, \quad (\text{A23})$$

corresponding exactly to the precise wavefunctions [24]. The relations in Eq. (A20) define implicitly the action-angle transformation from the real-space coordinates,

$$I_j = \Lambda_j(\vec{u}, \vec{p}, t), \quad \theta_j = \Theta_j(\vec{u}, \vec{p}, t), \quad (\text{A24})$$

with the transformation functions Λ_j and Θ_j depending explicitly on time (and being π -periodic), and can be constructed explicitly using Eq. (A20) and Eq. (A17). In the following we will not need the functions Λ_j and Θ_j explicitly, however we will use the partial derivatives

$$\frac{\partial \Lambda_j}{\partial p_\alpha} = iU_{\alpha j} \xi_j - iU_{\alpha j}^* \chi_j, \quad \frac{\partial^2 \Lambda_j}{\partial p_\alpha \partial p_\beta} = U_{\alpha j} U_{\beta j}^* + U_{\alpha j}^* U_{\beta j}. \quad (\text{A25})$$

We note here that the entire derivation above would remain completely valid if Eq. (A7) is to be replaced by a more general time-reversal invariant and π -periodic linear system, i.e. a system of coupled Hill equations [20, 22, 24, 70], with higher harmonics of the fundamental frequency 2. In addition, we note that setting $\vec{C}_{2n}^j = \delta_{n,0} \vec{C}_0^j / (2\nu_j)^{1/2}$, the solutions for \vec{u} , \vec{p} reduce

to coupled harmonic oscillators with nondimensional frequencies ν_j . This is the pseudopotential approximation (within the harmonic approximation), with the motion described by the potential

$$V_{\text{h.o.}}(\vec{u}) = \frac{1}{2} \vec{u}^t N \vec{u}, \quad (\text{A26})$$

with N a time-independent coupling matrix.

Appendix B: The linear limit of cooling for a coupled Mathieu system

As derived in [15], a Fokker-Planck equation in D actions (equal to the space dimension) can be written using the probability flux vector \vec{S} whose components are given by

$$S_j(\vec{I}, t) \equiv \Pi_j P - \frac{1}{2} \sum_k \frac{\partial}{\partial I_k} [\Pi_{jk} P], \quad (\text{B1})$$

with the FP equation taking the form

$$\begin{aligned} \frac{\partial P(\vec{I}, t)}{\partial t} &= - \sum_j \frac{\partial S_j(\vec{I}, t)}{\partial I_j} = \\ &= - \sum_j \frac{\partial}{\partial I_j} [\Pi_j P] + \frac{1}{2} \sum_{j,k} \frac{\partial^2}{\partial I_j \partial I_k} [\Pi_{jk} P]. \end{aligned} \quad (\text{B2})$$

For a multidimensional torus, generalizing Eq. (55), a phase-space point is defined by

$$Z_a \equiv \{\vec{u}, \vec{p}, t\}, \quad (\text{B3})$$

and defining the torus average over any function $\Xi(\vec{I}, \vec{\theta}, t)$ of the phase space, where Ξ is assumed to have an arbitrary period T ,

$$\Xi(\vec{I}, \vec{\theta}, t + T) = \Xi(\vec{I}, \vec{\theta}, t), \quad (\text{B4})$$

we have

$$\bar{\Xi}(\vec{I}) \equiv \frac{1}{T} \int_0^T dt \frac{1}{(2\pi)^D} \int \Xi(\vec{I}, \vec{\theta}, t) d^D \vec{\theta}, \quad (\text{B5})$$

with the adiabaticity conditions,

$$\Pi_j(\vec{I})/\nu_j \ll I_j, \quad \Pi_{jk}(\vec{I})/\sqrt{\nu_j \nu_k} \ll I_j I_k. \quad (\text{B6})$$

The mean drift and diffusion rates are given by

$$\Pi_j(\vec{I}) = \Gamma \overline{\rho(Z_a) \langle \delta I_j \rangle}, \quad \Pi_{jk}(\vec{I}) = \Gamma \overline{\rho(Z_a) \langle \delta I_j \delta I_k \rangle}, \quad (\text{B7})$$

with

$$\begin{aligned} \langle \delta I_j \rangle &= p_r \sum_\alpha \hat{k}_\alpha \frac{\partial \Lambda_j(Z_a)}{\partial p_\alpha} \\ &+ \frac{1}{2} p_r^2 \sum_{\alpha, \beta} \left[\hat{k}_\alpha \hat{k}_\beta \frac{\partial^2 \Lambda_j(Z_a)}{\partial p_\alpha \partial p_\beta} + \mu_{\alpha\beta} \left\langle \frac{\partial^2 \Lambda_j(Z_a)}{\partial p_\alpha \partial p_\beta} \right\rangle_\Gamma \right], \end{aligned} \quad (\text{B8})$$

and

$$\langle \delta I_j \delta I_k \rangle = p_r^2 \sum_{\alpha, \beta} \left[\hat{k}_\alpha \hat{k}_\beta \frac{\partial \Lambda_j}{\partial p_\alpha} \frac{\partial \Lambda_k}{\partial p_\beta} + \mu_{\alpha\beta} \left\langle \frac{\partial \Lambda_j}{\partial p_\alpha} \frac{\partial \Lambda_k}{\partial p_\beta} \right\rangle_\Gamma \right], \quad (\text{B9})$$

where all terms on the r.h.s above are functions of Z_a . The absorption probability for $s \ll 1$ takes the form of the Lorentzian $\rho = \sigma_{ee}^0$ of Eq. (35),

$$\rho(\vec{p}, t) = \frac{s/2}{1 + (2\Delta_{\text{eff}}/\Gamma)^2}, \quad \Delta_{\text{eff}} = \Delta - \vec{k} \cdot \vec{v}(\vec{p}, t), \quad (\text{B10})$$

with Δ_{eff} showing that $\vec{v}(\vec{p}, t)$ can be a function of the canonical momentum and time [Eq. (A5)].

Following the treatment of App. A we consider motion described by the coupled Mathieu system of Eq. (A7), and in this section we assume for simplicity that excess micromotion is negligible, i.e. we set

$$\vec{r}^0(t) = 0. \quad (\text{B11})$$

Under these conditions, that the velocities are small and that the potential is quadrupole, we can derive the following expressions for the linear limit of the cooling, which turns out to be identical within both the zero lifetime limit and the finite lifetime assumptions of the derivation.

Having assumed small velocities in this limit, we set $\vec{v} = \vec{p}$ in the rescaled units. Then, linearizing the Lorentzian in velocity we can write the coefficients in a well-known form [3, 10, 15],

$$p_r \Gamma \rho(\vec{p}) \approx F_r + \gamma \sum_{\beta} \hat{k}_\beta p_\beta, \quad (\text{B12})$$

with

$$F_r = \frac{p_r \Gamma s/2}{1 + (2\Delta/\Gamma)^2}, \quad \gamma = \frac{4k p_r s \Delta/\Gamma}{[1 + (2\Delta/\Gamma)^2]^2}. \quad (\text{B13})$$

Here F_r gives a mean radiation force (for $\vec{p} = 0$), and γ is a rate of damping. The condition for the validity of this linearization is

$$\vec{k} \cdot \vec{v} \ll [\Gamma^2 + 4\Delta^2]/(8|\Delta|). \quad (\text{B14})$$

Using Eqs. (A12), (A20) and (A25), the tori averages in Eq. (B7) would then contain bilinear terms of the oscillators $\vec{\xi}$ and $\vec{\chi}$. Let us assume first that the ion can be assumed stationary in space between the absorption and emission, which can be expressed by substituting

$$\Gamma e^{-\Gamma t'} \approx \delta(t') \quad (\text{B15})$$

in $\langle \cdot \rangle_\Gamma$ of Eq. (57). We will see below that the result without this restriction is in fact identical. Assuming that $\{\nu_j\}$ are nondegenerate [71], the only surviving combination will involve $\xi_j \chi_j$, due to Eq. (A21). We hence find that these terms become constants, or linear in the

actions. Defining the coefficients

$$c_{\alpha\beta}^j = \overline{(U_{\alpha j} U_{\beta j}^* + U_{\alpha j}^* U_{\beta j})}, \quad (\text{B16})$$

$$d_{\alpha\beta}^j = \overline{(iU_{\alpha j} V_{\beta j}^* - iU_{\alpha j}^* V_{\beta j})}, \quad (\text{B17})$$

allows us to put the FP coefficients in the form

$$\Pi_j^l(\vec{I}) = g_j I_j + h_j/2, \quad \Pi_{jk}^l(\vec{I}) = \tilde{h}_j I_j \delta_{j,k}, \quad (\text{B18})$$

with

$$g_j = \gamma \sum_{\alpha, \beta} \hat{k}_\alpha \hat{k}_\beta d_{\alpha\beta}^j, \quad h_j = \tilde{h}_j = \sum_{\alpha, \beta} D_{\alpha\beta}^l c_{\alpha\beta}^j, \quad (\text{B19})$$

and

$$D_{\alpha\beta}^l = p_r F_r (\hat{k}_\alpha \hat{k}_\beta + \mu_{\alpha\beta}). \quad (\text{B20})$$

We note that the fact that the same coefficient $h_j = \tilde{h}_j$ appears in both Π_j^l and Π_{jj}^l after the averaging (where they result from averaging different terms), is a consequence of the linearity of the oscillations, and is important in the following. In addition, for an isotropic laser, i.e. if $\hat{k}_\alpha = \hat{k}_\beta$, then Eq. (A16) implies that $g_j = \gamma$.

For a zero current state, with the probability flux vector defined in Eq. (B1), we require

$$\Pi_j^l P = \frac{1}{2} \frac{\partial}{\partial I_j} (\Pi_{jj}^l P). \quad (\text{B21})$$

Substituting the exponential ansatz

$$P = \left(\prod_j \lambda_j \right) \exp \left\{ - \sum_j \lambda_j I_j \right\}, \quad (\text{B22})$$

the zero-current condition becomes

$$g_j I_j + \frac{1}{2} h_j = \frac{1}{2} [\tilde{h}_j - \lambda_j \tilde{h}_j I_j], \quad (\text{B23})$$

and here we see that in order for the constant term to cancel on both sides of the equation, we must have $h_j = \tilde{h}_j$, i.e. the same coefficient in both the drift and the diffusion. The distribution is then solved by

$$\lambda_j = -2g_j/h_j. \quad (\text{B24})$$

This is a thermal-like, equilibrium distribution with mean action

$$\langle I_j \rangle = 1/\lambda_j, \quad (\text{B25})$$

provided that $g_j < 0$. This requires $\Delta < 0$ and also that none of the normal modes decouples from the laser.

Relaxing the instantaneous decay assumption of Eq. (B15), we now carry out the integration over the waiting time (exponential) distribution for decay from the excited level. The tori averages will result in terms which can be written in the form

$$\left\langle \frac{\partial \Lambda_j}{\partial p_\alpha} \frac{\partial \Lambda_k}{\partial p_\beta} \right\rangle_\Gamma = \sum \sqrt{I_j I_k} C_{2n}^{\alpha j} C_{2m}^{\beta j} \int_0^\pi \frac{1}{\pi} dt_a \int_0^{2\pi} \frac{1}{2\pi} d\phi_j \int_0^{2\pi} \frac{1}{2\pi} d\phi_k \int_0^\infty dt' \Gamma e^{-\Gamma t'} e^{i(\pm 2n \pm 2m \pm \nu_1 \pm \nu_2)(t_a + t')} e^{i(\pm \phi_j \pm \phi_k)}. \quad (\text{B26})$$

In the above integral, the order of integration does not matter, and hence the integration over t' can be performed last. In that case, the expression in Eq. (B26) reduces, by the arguments leading to Eq. (B16), to

$$\left\langle \frac{\partial \Lambda_j}{\partial p_\alpha} \frac{\partial \Lambda_k}{\partial p_\beta} \right\rangle_\Gamma = \int_0^\infty dt' \Gamma e^{-\Gamma t'} c_{\alpha\beta}^j I_j = c_{\alpha\beta}^j I_j, \quad (\text{B27})$$

and similarly,

$$\left\langle \frac{\partial^2 \Lambda_j}{\partial p_\alpha \partial p_\beta} \right\rangle_\Gamma = c_{\alpha\beta}^j. \quad (\text{B28})$$

This change of integration order does not hold (*a-priori*) if higher order terms in the Lorentzian expansion of Eq. (B12) have to be included, because they will appear outside of the dt' integration (the term linear in the momentum integrates to 0 in any case).

Hence the final stage of the cooling is described by an equilibrium distribution in the action coordinates, even when the ion cannot be treated as frozen between the absorption and emission, and even if it is driven by the high frequency rf trap to a large kinetic energy. Sufficient conditions for the validity of this approximation are the linearization [Eq. (B14)] and the nondegeneracy of the modes, in addition to the conditions of the derivation of the finite lifetime particle limit, presented in [15].

Appendix C: Cooling dynamics in 1D

1. Hamiltonian dynamics

Using the general derivation of App. A, the solution of the linear and homogeneous, Mathieu oscillator equation of motion derived from Eq. (39) is given by

$$u = \sqrt{I} (U(t)e^{i\theta} + U(t)^* e^{-i\theta}), \quad (\text{C1})$$

and

$$p = \sqrt{I} (V(t)e^{i\theta} + V(t)^* e^{-i\theta}). \quad (\text{C2})$$

The functions $U(t)$ and $V(t)$ are both π -periodic functions,

$$U(t) = \sum_n C_{2n} e^{i2nt}, \quad V(t) = i \sum_n C_{2n} (2n + \nu_z) e^{i2nt}, \quad (\text{C3})$$

and the normalization of the coefficients is given by

$$V(0)U(0) = \frac{1}{2}i. \quad (\text{C4})$$

The partial derivatives of the action angle transformation of Eq. (41) are given by

$$\frac{\partial \Lambda}{\partial p} = \sqrt{I} (iU(t)e^{i\theta} - iU(t)^* e^{-i\theta}), \quad \frac{\partial^2 \Lambda}{\partial^2 p} = 2|U(t)|^2. \quad (\text{C5})$$

For the particular solution of the inhomogenous equation derived from V_e of Eq. (36), we can substitute \bar{z} of Eq. (37), obtaining the recursion relations

$$[B_{2n}(a_z - 4n^2) - q_z(B_{2n-2} + B_{2n+2})] = E_z \delta_{n,0}. \quad (\text{C6})$$

To get a continued fraction expansion we use the assumed time-reversal invariance of the solution, $B_{2n} = B_{-2n}$, and define $c_{2n} = B_{2n+2}/B_{2n}$, getting $c_{2n-2}c_{2n} = B_{2n+2}/B_{2n-2}$, so

$$B_0 = E_z/(a_z - 2q_z c_0), \quad (\text{C7})$$

$$c_{2n-2} = q_z/(a_z - 4n^2 - q_z c_{2n}), \quad n \geq 1. \quad (\text{C8})$$

To the leading order [Eq. (45)] we have for the coefficients of \bar{z} ,

$$B_0 \approx E_z/\nu_z, \quad B_2 \approx -B_0 q_z/4, \quad B_4 \approx 0. \quad (\text{C9})$$

2. Low-Frequency Excess Micromotion

In the absence of excess micromotion, the final stage of the cooling in the Mathieu oscillator potential has been studied in [15] and here, above. We now generalize this treatment to include excess micromotion in the limit of Eq. (34) [with a micromotion frequency smaller than the excited state linewidth], focusing on 1D motion.

We assume that the low-frequency micromotion Lorentzian $\rho = \sigma_{ee}^0$ of Eq. (35) can be expanded in the velocity, subject to conditions of validity that will be elucidated later. We carry the expansion to third order in v_z , and then we set $v_z = \dot{z} + p$ in the rescaled units (with the mass set to 1), and assume in addition that p remains small, obtaining

$$p_r \Gamma \rho \approx F_r + \gamma v_z + \kappa v_z^2 \approx F_r + \gamma \dot{z} + \kappa \dot{z}^2 + \gamma p, \quad (\text{C10})$$

with F_r and γ defined in Eq. (72), and the nonlinear damping coefficient is

$$\kappa = \frac{2k^2 p_r s (1 - 12(\Delta/\Gamma)^2)/\Gamma}{[1 + (2\Delta/\Gamma)^2]^3}. \quad (\text{C11})$$

Plugging Eq. (C10) and Eq. (C5) into Eqs. (53)-(54), using Eq. (A16) and performing the averaging of Eq. (B5)

by exploiting the fact that the order of the integration of the exponential decay of Eq. (57) can be interchanged with the averaging in this limit of linearization [App. B], we get

$$\Pi_I = \gamma I + j_z/2, \quad \Pi_{II} = j_z I, \quad (\text{C12})$$

where the coefficient of excess micromotion is

$$j_z = p_r(1 + \mu)(F_r c_z + \gamma d_z + \kappa e_z), \quad (\text{C13})$$

with

$$c_z = \overline{|U|^2}, \quad (\text{C14})$$

and

$$d_z = \overline{2\dot{z}|U|^2}, \quad e_z = \overline{2\dot{z}^2|U|^2}. \quad (\text{C15})$$

We note that j_z generalizes i_z of Eq. (71) (for which d_z and e_z both vanish), which generalizes a similar coefficient for the harmonic oscillator, h_z defined in [15], for which c_z is replaced by ν_z^{-1} . Since \dot{z} , given in Eq. (49), is odd under time-reversal, while $|U(t)|^2 = U(t)U(t)^*$ is even (as $U(t)$ is a sum of exponentials), we see that $d_z = 0$, so the leading order correction to the action distribution is in second order in the excess micromotion amplitude A_z defined in Eq. (48). We can also see from the expression of κ that this correction is negative for $\Delta < -\sqrt{1/12}$. For $\Delta \lesssim -0.8\Gamma$ we find that the curves of the final action $\langle I \rangle$ as a function of A_z have indeed a negative derivative and decrease (initially) as the micromotion is increased from $A_z = 0$. This result does not hold for smaller detunings, for which the mean action always increases, because of higher order terms and the fact that the condition for the validity of this expansion does not accurately hold. The Taylor expansion of the Lorentzian as in Eq. (C10) is relevant subject to the condition

$$\max v_z \approx A_z \ll [\Gamma^2 + 4\Delta^2]/(8k|\Delta|), \quad (\text{C16})$$

which defines a curve $A_{\text{linear}}(\Delta)$ shown in Fig. 4. For A_z obeying this condition, the effect of the micromotion vanishes at first order in A_z , and it is small effect overall. In addition, since the term proportional to κ was evaluated based on assuming also $p \ll \dot{z}$, its relevance requires also that

$$I \ll A_z^2/(12\nu_z), \quad (\text{C17})$$

(where the numerical factor 12 is approximate), which does not hold for A_z too small. This is why for $-0.8 \lesssim \Delta/\Gamma < 0$, Eq. (C16) and Eq. (C17) cannot be satisfied together, and indeed we find that $\langle I \rangle$ monotonously increases as a function of A_z for these detunings (instead of decreasing initially).

Appendix D: Excess micromotion Expanded in terms of Bessel functions

To connect our Floquet approach with the excess micromotion treatment of [17–19], starting from the OBE in the form of Eqs. (8)-(9), we can make a different substitution than that of Eq. (10),

$$\sigma'_{ge} = e^{-i\omega_L t} \sigma_{ge}, \quad (\text{D1})$$

obtaining, to first order in Ω_R , the OBE in the form

$$\dot{\sigma}_{ee} = -\Gamma \sigma_{ee} - i \frac{\Omega_R}{2} (e^{-i\phi} \sigma'_{ge} - e^{i\phi} \sigma'_{eg}), \quad (\text{D2})$$

$$\dot{\sigma}'_{ge} = \left(i\Delta - \frac{\Gamma}{2} \right) \sigma'_{ge} + i \frac{\Omega_R}{2} e^{i\phi}. \quad (\text{D3})$$

Writing the phase in the following form (setting $\phi_L = 0$),

$$\phi = -\vec{k} \cdot \vec{r}(t) = \beta \cos(2t), \quad (\text{D4})$$

amounts to an expansion of the excess micromotion but not the perturbations about it. We have

$$e^{i\phi} = \sum_n i^n J_n(\beta) e^{i2nt}. \quad (\text{D5})$$

Expanding again

$$\sigma'_{ge} = \sum_n G_{2n} e^{i2nt}, \quad (\text{D6})$$

we have

$$i \sum_n 2n G_{2n} e^{i2nt} = \left(i\Delta - \frac{\Gamma}{2} \right) \sum_n G_{2n} e^{i2nt} + i \frac{\Omega_R}{2} \sum_n i^n J_n(\beta) e^{i2nt}, \quad (\text{D7})$$

which implies

$$G_{2n} = \frac{i^{n+1}(\Omega_R/2)J_n(\beta)}{i(2n - \Delta) + \Gamma/2} = \frac{i^{n+1}(\Omega_R/2)J_n(\beta) [\Gamma/2 - i(2n - \Delta)]}{(2n - \Delta)^2 + (\Gamma/2)^2}. \quad (\text{D8})$$

We have

$$e^{-i\phi} \sigma'_{ge} = \sum_{m,n} i^{-m} J_m(\beta) e^{-i2mt} G_{2n} e^{i2nt} = \sum_{m,p} i^{-m} J_m(\beta) G_{2(m+p)} e^{i2pt}, \quad (\text{D9})$$

and substitution in Eq. (D2) gives

$$\dot{\sigma}_{ee} = -\Gamma \sigma_{ee} + \Omega_R \text{Im} \left(\sum_{m,p} i^{-m} J_m(\beta) G_{2(m+p)} e^{i2pt} \right). \quad (\text{D10})$$

Expanding,

$$\sigma_{ee} = \text{Im} \sum_n \rho_{2n} e^{i2nt}, \quad (\text{D11})$$

we have

$$\dot{\sigma}_{ee} = \text{Im} \sum_n i2n \rho_{2n} e^{i2nt}, \quad (\text{D12})$$

and substitution in Eq. (D10) gives

$$i2n \rho_{2n} = -\Gamma \rho_{2n} + \Omega_R \sum_m i^{-m} J_m(\beta) G_{2(m+n)}, \quad (\text{D13})$$

which can be solved for all n . For the stationary component $n = 0$, we get

$$\rho_0 = \frac{\Omega_R}{\Gamma} \sum_m i^m J_m(\beta) G_{2m}, \quad (\text{D14})$$

and the known result for the averaged absorption probability over a micromotion-period (as mentioned in [17]),

$$\rho_0 = \frac{\Omega_R^2}{4} \sum_m \frac{J_m(\beta)^2}{(2m - \Delta)^2 + (\Gamma/2)^2}. \quad (\text{D15})$$

-
- [1] Wolfgang Paul. Electromagnetic traps for charged and neutral particles. *Reviews of modern physics*, 62(3):531, 1990.
- [2] David J Wineland and Wayne M Itano. Laser cooling of atoms. *Physical Review A*, 20(4):1521, 1979.
- [3] J. Javanainen. Light-pressure cooling of trapped ions in three dimensions. *Applied Physics*, 23(2):175–182, 10 1980.
- [4] J. Javanainen and S. Stenholm. Laser cooling of trapped particles i: The heavy particle limit. *Applied Physics*, 21(3):283–291, 03 1980.
- [5] Juha Javanainen and Stig Stenholm. Laser cooling of trapped particles ii. *Applied Physics A: Materials Science & Processing*, 24(1):71–84, 1981.
- [6] JP Gordon and A Ashkin. Motion of atoms in a radiation trap. *Physical Review A*, 21(5):1606, 1980.
- [7] Stig Stenholm. The semiclassical theory of laser cooling. *Reviews of modern physics*, 58(3):699, 1986.
- [8] JI Cirac, LJ Garay, R Blatt, AS Parkins, and P Zoller. Laser cooling of trapped ions: The influence of micromotion. *Physical review A*, 49(1):421, 1994.
- [9] Marek Šašura and Vladimír Bužek. Cold trapped ions as quantum information processors. *journal of modern optics*, 49(10):1593–1647, 2002.
- [10] D. Leibfried, R. Blatt, C. Monroe, and D. Wineland. Quantum dynamics of single trapped ions. *Reviews of Modern Physics*, 75(1):281–324, 2003.
- [11] J. H. Wesenberg, R. J. Epstein, D. Leibfried, R. B. Blakestad, J. Britton, J. P. Home, W. M. Itano, J. D. Jost, E. Knill, C. Langer, R. Ozeri, S. Seidelin, and D. J. Wineland. Fluorescence during doppler cooling of a single trapped atom. *Physical Review A*, 76(5), 11 2007.
- [12] R. J. Epstein, S. Seidelin, D. Leibfried, J. H. Wesenberg, J. J. Bollinger, J. M. Amini, R. B. Blakestad, J. Britton, J. P. Home, W. M. Itano, J. D. Jost, E. Knill, C. Langer, R. Ozeri, N. Shiga, and D. J. Wineland. Simplified motional heating rate measurements of trapped ions. *Physical Review A*, 76(3), 09 2007.
- [13] M. Marciante, C. Champenois, A. Calisti, J. Pedregosa-Gutierrez, and M. Knoop. Ion dynamics in a linear radio-frequency trap with a single cooling laser. *Physical Review A*, 82(3), 09 2010.
- [14] Tomas Sikorsky, Ziv Meir, Nitzan Akerman, Ruti Benschlomi, and Roe Ozeri. Doppler cooling thermometry of a multilevel ion in the presence of micromotion. *Phys. Rev. A*, 96:012519, Jul 2017.
- [15] A Maitra, D Leibfried, D Ullmo, and H Landa. Far-from-equilibrium noise heating and laser cooling dynamics in radio-frequency paul traps. *arXiv preprint arXiv:1808.07816*, 2018.
- [16] Lionel Podlecki, RD Glover, John Martin, and Thierry Bastin. Radiation pressure on a two-level atom: an exact analytical approach. *JOSA B*, 35(1):127–132, 2018.
- [17] RG DeVoe, J Hoffnagle, and RG Brewer. Role of laser damping in trapped ion crystals. *Physical Review A*, 39(9):4362, 1989.
- [18] R. Blümel, C. Kappler, W. Quint, and H. Walther. Chaos and order of laser-cooled ions in a Paul trap. *Phys. Rev. A*, 40(2):808–823, Jul 1989.
- [19] DJ Berkeland, JD Miller, James C Bergquist, Wayne M Itano, and David J Wineland. Minimization of ion micromotion in a paul trap. *Journal of applied physics*, 83(10):5025–5033, 1998.
- [20] N. W. McLachlan. *Theory and Applications of Mathieu Functions*. Clarendon, Oxford, 1947.
- [21] A. Maitra, D. Leibfried, D. Ullmo, and H. Landa. Can a periodically driven particle resist laser cooling and noise? *arXiv preprint arXiv:1810.01856*, 2018.
- [22] H. Landa, M. Drewsen, B. Reznik, and A. Retzker. Modes of oscillation in radiofrequency Paul traps. *New Journal of Physics*, 14(9):093023, 2012.
- [23] G. Grynberg, A. Aspect, C. Fabre, and C. Cohen-Tannoudji. *Introduction to Quantum Optics: From the Semi-classical Approach to Quantized Light*. Cambridge University Press, 2010.
- [24] H Landa, M Drewsen, B Reznik, and A Retzker. Classical and quantum modes of coupled mathieu equations. *Journal of Physics A: Mathematical and Theoretical*, 45(45):455305, 2012.
- [25] V. Roberdel, D. Leibfried, D. Ullmo, and H. Landa. Phase-space study of surface-electrode paul traps: Integrable, chaotic, and mixed motions. *Phys. Rev. A*, 97:053419, May 2018.
- [26] H. Kaufmann, S. Ulm, G. Jacob, U. Poschinger, H. Landa, A. Retzker, M. B. Plenio, and F. Schmidt-Kaler. Precise experimental investigation of eigenmodes in a planar ion crystal. *Phys. Rev. Lett.*, 109:263003, Dec 2012.
- [27] Marie Chupeau, Sergio Ciliberto, David Guéry-Odelin, and Emmanuel Trizac. Engineered swift equilibration

- for brownian objects: from underdamped to overdamped dynamics. *New Journal of Physics*, 2018.
- [28] Giovanna Morigi and Jürgen Eschner. Doppler cooling of a coulomb crystal. *Phys. Rev. A*, 64:063407, Nov 2001.
- [29] Giovanna Morigi and Jürgen Eschner. Is an ion string laser-cooled like a single ion? *Journal of Physics B: Atomic, Molecular and Optical Physics*, 36(5):1041, 2003.
- [30] G. Morigi and H. Walther. Two-species coulomb chains for quantum information. *The European Physical Journal D-Atomic, Molecular, Optical and Plasma Physics*, 13(2):261–269, 2001.
- [31] Thomás Fogarty, Haggai Landa, Cecilia Cormick, and Giovanna Morigi. Optomechanical many-body cooling to the ground state using frustration. *Physical Review A*, 94(2):023844, 2016.
- [32] Thomas Lauprêtre, Rasmus B Linnet, Ian D Leroux, Haggai Landa, Aurélien Dantan, and Michael Drewsen. Controlling the potential landscape and normal modes of ion coulomb crystals by a standing-wave optical potential. *Physical Review A*, 99(3):031401, 2019.
- [33] Marius Romuald Kamsap, Caroline Champenois, J Pedregosa-Gutierrez, Simon Mahler, Marie Houssin, and Martina Knoop. Experimental demonstration of an efficient number diagnostic for long ion chains. *Physical Review A*, 95(1):013413, 2017.
- [34] S. Ejtemaee and P. C. Haljan. 3d sisyphus cooling of trapped ions. *Phys. Rev. Lett.*, 119:043001, Jul 2017.
- [35] Cecilia Cormick, Tobias Schaetz, and Giovanna Morigi. Trapping ions with lasers. *New Journal of Physics*, 13(4):043019, 2011.
- [36] Julian Schmidt, Alexander Lambrecht, Pascal Weckesser, Markus Debatin, Leon Karpa, and Tobias Schaetz. Optical trapping of ion coulomb crystals. *Phys. Rev. X*, 8:021028, May 2018.
- [37] T. B. Mitchell, J. J. Bollinger, D. H. E. Dubin, X.-P. Huang, W. M. Itano, and R. H. Baughman. Direct observations of structural phase transitions in planar crystallized ion plasmas. *Science*, 282(5392):1290–1293, 1998.
- [38] A. Mortensen, E. Nielsen, T. Matthey, and M. Drewsen. Observation of three-dimensional long-range order in small ion coulomb crystals in an rf trap. *Phys. Rev. Lett.*, 96(10):103001, Mar 2006.
- [39] A. Ostendorf, C. B. Zhang, M. A. Wilson, D. Offenber, B. Roth, and S. Schiller. Sympathetic cooling of complex molecular ions to millikelvin temperatures. *Phys. Rev. Lett.*, 97:243005, Dec 2006.
- [40] B Szymanski, R Dubessy, B Dubost, S Guibal, J-P Likhforman, and L Guidoni. Large two dimensional coulomb crystals in a radio frequency surface ion trap. *Applied Physics Letters*, 100(17):171110, 2012.
- [41] DA Tabor, V Rajagopal, Y-W Lin, and B Odom. Suitability of linear quadrupole ion traps for large coulomb crystals. *Applied Physics B*, 107(4):1097–1104, 2012.
- [42] Sandeep Mavadia, Joseph F Goodwin, Graham Stutter, Shailen Bharadia, Daniel R Crick, Daniel M Segal, and Richard C Thompson. Control of the conformations of ion coulomb crystals in a penning trap. *Nature communications*, 4:2571, 2013.
- [43] Justin G Bohnet, Brian C Sawyer, Joseph W Britton, Michael L Wall, Ana Maria Rey, Michael Foss-Feig, and John J Bollinger. Quantum spin dynamics and entanglement generation with hundreds of trapped ions. *Science*, 352(6291):1297–1301, 2016.
- [44] Claude Godrèche and Jean-Marc Luck. Characterizing the nonequilibrium stationary states of ornstein–uhlenbeck processes. *Journal of Physics A: Mathematical and Theoretical*, 52(3):035002, 2018.
- [45] H Janacek, AM Steane, DM Lucas, and DN Stacey. The effect of atomic response time in the theory of doppler cooling of trapped ions. *Journal of Modern Optics*, 65(5-6):577–584, 2018.
- [46] Ralph G DeVoe. Power-law distributions for a trapped ion interacting with a classical buffer gas. *Physical review letters*, 102(6):063001, 2009.
- [47] I Rouse and S Willitsch. Superstatistical energy distributions of an ion in an ultracold buffer gas. *Physical review letters*, 118(14):143401, 2017.
- [48] I Rouse and S Willitsch. Energy distributions of an ion in a radio-frequency trap immersed in a buffer gas under the influence of additional external forces. *Physical Review A*, 97(4):042712, 2018.
- [49] Ziv Meir, Meirav Pinkas, Tomas Sikorsky, Ruti Benschlomi, Nitzan Akerman, and Roei Ozeri. Direct observation of atom-ion non-equilibrium sympathetic cooling. *arXiv preprint arXiv:1801.06839*, 2018.
- [50] Q. A. Turchette, C. S. Wood, B. E. King, C. J. Myatt, D. Leibfried, W. M. Itano, C. Monroe, and D. J. Wineland. Deterministic entanglement of two trapped ions. *Phys. Rev. Lett.*, 81:3631–3634, Oct 1998.
- [51] A. Retzker, R. C. Thompson, D. M. Segal, and M. B. Plenio. Double well potentials and quantum phase transitions in ion traps. *Phys. Rev. Lett.*, 101:260504, Dec 2008.
- [52] H. Landa, A. Retzker, T. Schaetz, and B. Reznik. Entanglement Generation Using Discrete Solitons in Coulomb Crystals. *Phys. Rev. Lett.*, 113:053001, 2014.
- [53] C. Shen and L.-M. Duan. High-fidelity quantum gates for trapped ions under micromotion. *Phys. Rev. A*, 90:022332, Aug 2014.
- [54] S-T Wang, Chao Shen, and L-M Duan. Quantum computation under micromotion in a planar ion crystal. *Scientific reports*, 5:8555, 2015.
- [55] Kyle Arnold, Elnur Hajiyev, Eduardo Paez, Chern Hui Lee, MD Barrett, and John Bollinger. Prospects for atomic clocks based on large ion crystals. *Physical Review A*, 92(3):032108, 2015.
- [56] J Keller, HL Partner, T Burgermeister, and TE Mehlstäubler. Precise determination of micromotion for trapped-ion optical clocks. *Journal of Applied Physics*, 118(10):104501, 2015.
- [57] LL Yan, W Wan, L Chen, F Zhou, SJ Gong, X Tong, and M Feng. Exploring structural phase transitions of ion crystals. *Scientific reports*, 6:21547, 2016.
- [58] Manuel Mielenz, Henning Kalis, Matthias Wittemer, Frederick Hakelberg, Ulrich Warring, Roman Schmied, Matthew Blain, Peter Maunz, David L Moehring, Dietrich Leibfried, et al. Arrays of individually controlled ions suitable for two-dimensional quantum simulations. *Nature communications*, 7:ncomms11839, 2016.
- [59] Colin D Bruzewicz, Robert McConnell, John Chiaverini, and Jeremy M Sage. Scalable loading of a two-dimensional trapped-ion array. *Nature communications*,

- 7:13005, 2016.
- [60] J Keller, D Kalincev, T Burgermeister, A Kulosa, A Didier, T Nordmann, J Kiethe, and TE Mehlstäubler. Optical clocks based on linear ion chains with high stability and accuracy. *arXiv preprint arXiv:1712.02335*, 2017.
- [61] J Keller, T Burgermeister, D Kalincev, A Didier, AP Kulosa, T Nordmann, J Kiethe, and TE Mehlstäubler. Controlling systematic frequency uncertainties at the 10^{-19} level in linear coulomb crystals. *arXiv preprint arXiv:1803.08248*, 2018.
- [62] J Welzel, F Stopp, and F Schmidt-Kaler. Spin and motion dynamics with zigzag ion crystals in transverse magnetic field gradients. *arXiv preprint arXiv:1801.03391*, 2018.
- [63] Marion Delehaye and Clément Lacroûte. Single-ion, transportable optical atomic clocks. *Journal of Modern Optics*, 65(5-6):622–639, 2018.
- [64] Yukai Wu, Sheng-Tao Wang, and L.-M. Duan. Noise analysis for high-fidelity quantum entangling gates in an anharmonic linear paul trap. *Phys. Rev. A*, 97:062325, Jun 2018.
- [65] R. J. Glauber. *Laser manipulation of atoms and ions: proceedings of the International School of Physics "Enrico Fermi", course 118, edited by E. Arimondo, W. D. Phillips, and F. Strumia*. North-Holland, Amsterdam, 1992.
- [66] Bogdan M Mihalcea. Study of quasiclassical dynamics of trapped ions using the coherent state formalism and associated algebraic groups. *Romanian Journal of Physics*, 62:113, 2017.
- [67] C. Champenois, M. Marciante, J. Pedregosa-Gutierrez, M. Houssin, M. Knoop, and M. Kajita. Ion ring in a linear multipole trap for optical frequency metrology. *Phys. Rev. A*, 81:043410, Apr 2010.
- [68] Fayaz A Shaikh and Arkadas Ozakin. Stability analysis of ion motion in asymmetric planar ion traps. *Journal of Applied Physics*, 112(7):074904, 2012.
- [69] O Bohigas, S Tomsovic, and D Ullmo. Manifestations of classical phase space structures in quantum mechanics. *Physics Reports*, 223(2):133–43, 01 1993.
- [70] V. A. Yakubovich and V. M. Starzhinskii. *Linear Differential Equations with Periodic Coefficients*. John Wiley and Sons, 1975.
- [71] For an analysis of laser-induced correlations between two nearly-degenerate harmonic oscillator modes, see [3].